

# A Two-Phase Model to Investigate LDL Toxicity in Early Atherosclerosis

Abdush Salam Pramanik<sup>1</sup>, Bibaswan Dey<sup>1\*</sup>, G. P. Raja Sekhar<sup>2</sup>

<sup>1</sup>Department of Mathematics, University of North Bengal, Raja Rammohunpur, Darjeeling, 734013, West Bengal, India.

<sup>2</sup>Department of Mathematics, Indian Institute of Technology Kharagpur, Kharagpur, 721302, West Bengal, India.

\*Corresponding author(s). E-mail(s): [bibaswandey@nbu.ac.in](mailto:bibaswandey@nbu.ac.in);  
Contributing authors: [rs\\_abdush@nbu.ac.in](mailto:rs_abdush@nbu.ac.in); [rajas@iitkgp.ac.in](mailto:rajas@iitkgp.ac.in);

## Abstract

Atherosclerosis is a chronic inflammatory cardiovascular disease in which fatty plaque is built inside an artery wall. Early atherosclerotic plaque development is typically characterised by inflammatory tissues primarily consisting of foam cells and macrophages. We present a multiphase model that explores early plaque growth to emphasise the role of cytokines (in particular, Monocyte Chemoattractant Protein-1) and oxidised low-density lipoprotein (oxLDL) in monocyte recruitment and foam cell production, respectively. The plaque boundary is assumed to move at the same speed as the inflammatory tissues close to the periphery. This study discusses oxLDL-induced toxic environment towards macrophages and foam cells such that they start to die beyond a threshold limit of oxLDL concentration owing to excessive consumption. Our findings reveal that initially, the plaque evolves rapidly, and the growth rate subsequently reduces because of oxLDL-induced toxicity. In addition, it is observed that the saturation of inflammatory cell volume fraction becomes independent of oxLDL concentration beyond the threshold limit, referred to as the oxLDL toxicity limit. Our study manifests that increased oxLDL and cytokines influx promotes stable plaque growth through oxLDL-induced toxicity, while elevated cytokines outflux disrupts the stability. Detailed analysis of the model presented in this article unfolds critical insights into the various biochemical and cellular mechanisms behind early plaque development.

**Keywords:** Oxidised LDL (oxLDL), Functional Cytokines (f-cytokines), Macrophage, Foam Cell, Perturbation Approximation, Mixture Theory

# 1 Introduction

Cardiovascular diseases (CVDs) have become a major warning to human health and a leading cause of loss of life worldwide (Roth et al, 2018). Atherosclerosis, a type of CVD, is an inflammatory disease associated with an excess concentration of low-density lipoprotein (LDL) in the bloodstream. Typical risk factors such as hypertension, smoking, diabetes, hyperlipidemia, etc., can result in a dreadful situation for a person having atherosclerosis (Cunningham and Gotlieb, 2005). Primarily, atherosclerosis occurs within bifurcated large and medium arteries, particularly at the position of curvature where a low value of endothelium shear stress is anticipated (Chatzizisis et al, 2007). The plaque formation begins with the deposition of sizeable lipid-laden foam cells derived from monocytes which phagocyte oxidized low-density lipoprotein (oxLDL) present within intima (Libby et al, 2002). In due course of time, such a plaque becomes stiff and unstable so that it can rupture. Subsequently, blood clots develop at the ruptured portion of the plaque and can block blood flow, resulting in myocardial infarction, ischemic cerebral stroke, etc. (Hansson and Libby, 2006). Plaque formation is almost asymptomatic in a patient with atherosclerosis unless diagnosed clinically (Davies and Woolf, 1993). Hence it is essential to detect the plaque at an early stage in order to prevent above mentioned fatal health complications. Therefore, a complete understanding of plaque growth in early atherosclerosis is crucial.

Early atherosclerotic plaque develops in the narrow intimal layer of an artery. Fig. 1 depicts the layered structure of a healthy artery wall. When there is turbulence of recirculation in the blood flow into the lumen region, the endothelium gets damaged, particularly in areas of low shear stress. Several factors, such as hypertension, smoking, consuming processed foods and alcohol etc., expedite endothelium damage (Channon, 2006; Furchgott, 1999). Low-density lipoprotein (LDL) from the bloodstream penetrates the artery wall to enter the intima through the injured endothelium. Inside intima, LDL molecules are modified by free oxygen radicals to become oxidized LDL (oxLDL) (Lusis, 2000; Cobbold et al, 2002). The presence of oxLDL enables endothelium cells to secrete monocyte chemoattractant protein-1 (MCP-1) and monocyte colony-stimulating factor (M-CSF) (Wu et al, 2017). In addition, the endothelium in the vicinity of oxLDL expresses leukocyte adhesion molecules on the surface of the endothelium, such as vascular cell adhesion molecule-1 (VCAM-1) and intracellular adhesion molecules (ICAM-1) (Libby et al, 2002; Hansson and Libby, 2006). These adhesion molecules allow monocytes from the bloodstream to attach to the endothelium surface (Lusis, 2000). The monocytes enter the intima in response to chemoattractant gradients like MCP-1 and other cytokines (Han et al, 2004; Hansson and Libby, 2006; Lusis, 2000). Subsequently, monocytes differentiate into macrophages inside the intima in response to M-CSF (Ross, 1999; Libby et al, 2002). Macrophages within the intima consume oxLDL, which causes them to become large, lipid-laden foam cells (Lusis, 2000; Calvez et al, 2009; Gui et al, 2012; Hao and Friedman, 2014). Consequently, several foam cells produced with macrophages form an early plaque in atherosclerosis (Chalmers et al, 2015). At this early stage (early atherosclerosis), two essential components of the formed plaque are foam cells and macrophages. These foam cells further secrete more chemoattractants and cytokines

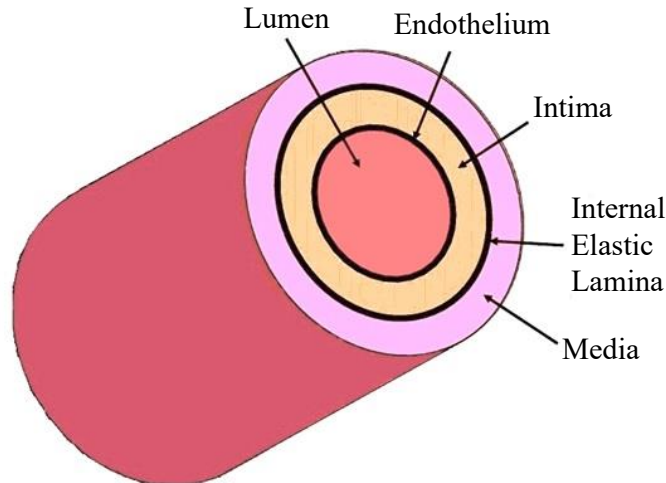


**Fig. 1:** Cross-section of a healthy artery showing the artery wall consists of different cell layers. The innermost layer of the wall is comprised of a thin sheet of endothelium cells, called *the endothelium*. The endothelium forms an interface between the blood flow in the lumen and the rest of the artery wall. Immediately beneath the endothelium, a thin tissue layer lies called the *intima*. The underlying tissue layer is said to be *media* which is separated from the intima by a dense tissue membrane known as *internal elastic lamina (IEL)*.

to attract more monocytes into the intima (Chalmers et al, 2017; Ross, 1999). Although the death of macrophages and foam cells is not excessively studied, some studies describe the possible cause of death. According to Marchant et al (1996), macrophages die due to the toxic environment induced by oxLDL. In addition, foam cells die due to the extensive consumption of oxLDL (Hegyí et al, 1996; Liu et al, 2008). Consequently, a threshold value of oxLDL concentration exists, after which inflammatory cells (macrophages, foam cells) start to die (Liu et al, 2008). The dead foam cells within plaque release oxLDL and other cellular debris (Berliner et al, 1995). Macrophages consume more oxLDL and produce new foam cells. Fig. 2 outlines the plaque formation at an early stage in a schematic diagram.

In the next stage, smooth muscle cells (SMCs) within the media region migrate through the IEL to the intima. The proliferation of SMCs is induced by growth factors like platelet-derived growth factor (PDGF) secreted from the endothelium and foam cells (Newby and Zaltsman, 1999). In addition, SMCs produce collagen, which is upregulated by a cytokine transforming growth factor-beta (TGF- $\beta$ ) released by foam cells, SMCs and endothelium cells (Hansson et al, 2006). Migrated SMCs and collagen contribute to the formation of a cap near the endothelium, referred to as the fibrous cap (Newby and Zaltsman, 1999). At this stage, the plaque becomes more arduous and is viewed as advanced atherosclerotic plaque. However, we intend to

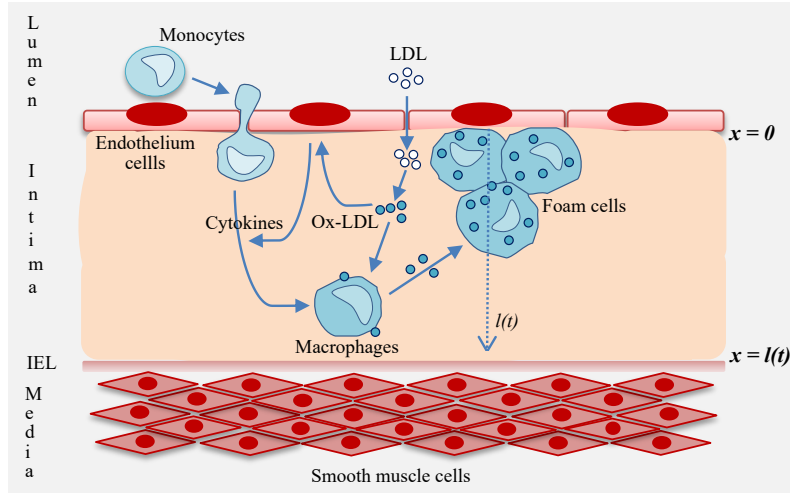


**Fig. 2:** Schematic diagram of the key processes in plaque formation at the early stage. Low-density lipoprotein (LDL), which is present in the bloodstream, enters the intima through the damaged endothelium and undergoes modification to become oxidized LDL (oxLDL). OxLDL induces the secretion of several cytokines from the endothelium cells, including monocyte chemoattractant protein-1 (MCP-1), monocyte colony-stimulating factor (M-CSF), and ES-cytokines. In response to the cytokines, particularly for MCP-1, monocytes adhere to the intima from the bloodstream and subsequently differentiate into macrophages. Within the intima, macrophages consume oxLDL to form large lipid-laden foam cells. The accumulation of foam cells produced by macrophages constitutes an early atherosclerotic plaque.

focus on early-stage plaque formation involving foam cells and macrophages. Hence, we aim to develop a mathematical model to describe plaque growth and the corresponding biochemical mechanism where the plaque boundary evolves with time.

Various mathematical models have been developed to understand the early stage of atherosclerosis with a specific focus. For example, [Cobbold et al \(2002\)](#) proposed a mathematical model for LDL oxidation using ordinary differential equations (ODEs) based on in-vitro experimental data. The presence of LDL, more precisely oxidized LDL, turns out to be a vital factor during the initial stage of atherosclerosis ([Navab et al, 2004](#)). In this regard, [Ibragimov et al \(2005\)](#) developed a model of early atherosclerotic lesion formation by a system of non-linear partial differential equations (PDEs) where the concentration of oxLDL is expressed through a diffusion-reaction equation. Numerous studies on the early stage of atherosclerosis used diffusion-reaction transport model for oxLDL concentration ([Calvez et al, 2009](#)) while some assume a constant transport ([Cohen et al, 2014](#)). The recruitment of monocytes from the lumen, their conversion to macrophages and finally, the production of foam cells from macrophages are necessary steps of plaque formation. Monocyte recruitment is initiated under the secretion of MCP-1 from the endothelium cells and differentiates

into macrophages under the influence of M-CSF. [Cilla et al \(2014\)](#) introduced a convection-diffusion type PDE of oxLDL concentration that incorporates the production and degradation of MCP-1. In general, the secretion of MCP-1 can be coupled with the chemoattractant M-CSF ([Ibragimov et al, 2005](#); [Filipovic et al, 2013](#)) as oxLDL is one of the critical factors behind atherosclerosis.

Monocyte recruitment and differentiation have been studied using simplified mathematical modellings where the governing equations describe the conversion of macrophages into foam cells after consuming oxLDL ([Calvez et al, 2009](#); [Cohen et al, 2014](#); [Chalmers et al, 2015](#)). [Ougrinovskaia et al \(2010\)](#) develops a simplified model at an early stage, including the uptake of oxLDL by macrophages to form foam cells. Their model assumes Michaelis-Menten kinetics for the uptake of oxLDL by macrophages, and the recruitment of macrophages depends on oxLDL. Moreover, they have used a sigmoidal function for saturating the uptake rate. In the model of [Cohen et al \(2014\)](#), the effect of HDL in the early stage of atherosclerosis has been included. Nevertheless, the rest of the equations are the same as in [Ougrinovskaia et al \(2010\)](#). [El Khatib et al \(2007, 2009, 2012\)](#) focus on plaque formation at an early stage of atherosclerosis where the density of monocytes and macrophages is represented as a system of reaction-diffusion equation. The presence of oxLDL draws monocytes or macrophages across the endothelium through nonlinear boundary conditions. A similar but more complicated model for early plaque formation has been proposed by [Calvez et al \(2009\)](#), which includes macrophages and oxLDL and a cytokine produced in response to the consumption of oxLDL by macrophages and prompts the recruitment of the monocyte at the endothelium. [Calvez et al \(2010\)](#) proposed an improved version of the previous model, coupled with a model for blood flow, to analyse how the distortion affects blood flow through the lumen region. [Chalmers et al \(2015\)](#) introduced a mathematical model of early atherosclerosis involving oxLDL, monocytes/macrophages, cytokines and foam cells to study the bifurcation analysis throughout the process.

Multiphase mixture theory has been widely used to model dynamic processes associated with biological tissues, remarkably heterogeneous tissues, for example, articular cartilage ([Mow et al, 1984](#)), solid tumor growth ([Breward et al, 2002](#); [Byrne et al, 2003](#); [Hubbard and Byrne, 2013](#)), hydrodynamics in solid tumor ([Dey and Raja Sekhar, 2016](#); [Dey et al, 2018](#); [Alam et al, 2019](#)), scaffold growth in tissue engineering ([Lemon et al, 2006](#); [Kumar et al, 2018](#)) and fluid injection into subcutaneous tissue ([Pramanik et al, 2023](#)). Recently [Watson et al \(2018\)](#) have employed the mixture theory approach to model early fibrous cap formation and smooth muscle cells (SMCs) migration corresponding to the advanced stage of atherosclerosis plaque formation. The SMCs are a significant part of the plaque, and the remaining part may be regarded as non-SMC. Later, [Watson et al \(2020\)](#) considered the plaque tissue a mixture of three distinct phases: SMC phase, collagen-rich fibrous extracellular matrix (ECM) and a generic tissue phase comprising the remaining plaque constituents. In addition, their study considers collagen cap formation by SMCs in response to diffusible growth factors like PDGF and TGF- $\beta$  from the endothelium.

Consequently, multiphase models produce a detailed description of plaque formation dynamics since they provide a natural framework for volume exclusion and mechanical interaction between plaque constituents. In this study, a multiphase approach is deployed as both volume exclusion, and mechanical interaction can play a crucial role in the plaque growth of early atherosclerosis.

In most of the above studies, the plaque material has been considered advanced and stable without apprising its overall growth. Consequently, the interface between the intima and media remains static. Hence, early plaque growth prediction may not be possible through those models. On the other hand, many researchers believe that atherosclerosis is an obvious application of free boundary models, but for various reasons, most ignore it. Recently, [Ahmed et al \(2023\)](#) developed a free boundary multiphase model corresponding to early atherosclerotic plaques to investigate the effects of impaired macrophage anti-inflammatory behaviour on plaque structure and its growth. The plaque is formed mainly by dead cells due to efferocytotic uptake by the macrophages. Motivated by the above developments of the atherosclerosis model, one can assume that the plaque boundary moves with a velocity equal to the speed of inflammatory tissue. The multiphase approach of the atherosclerosis model and moving plaque boundary can capture many mechanical and chemical features. For example, a tumor domain having free or moving boundary plays a significant role in the studies on tumor growth ([Breward et al, 2002, 2003](#)). This motivates us to investigate the model as a free boundary domain model.

This paper is structured through several sections. In the next section, we formulate a mathematical model based on the mixture theory, assuming atherosclerotic plaque is a two-phase material composed of inflammatory and non-inflammatory tissues. Further, governing equations for the plaque growth are simplified for a 1D cartesian geometry. The governing equations are nonlinear due to the underlying physics; however, the Michaelis–Menten general kinetics corresponding to the oxLDL metabolism by macrophages is highly significant. In order to linearize the oxLDL transport equation, a perturbation expansion method is deployed by assuming the weak nonlinear nature of the oxLDL metabolism. Subsequently, the finite difference method is applied to the resulting leading and first-order equations satisfying the CFL condition. The novel feature of this study is the use of a combination of perturbation and numerical methods for efficiently handling the nonlinearity related to the oxLDL metabolism by macrophage.

## 2 Mathematical Formulation

To model the growth of an early-stage atherosclerotic plaque, we hypothesize that it is caused by the accumulation of macrophages and foam cells. Indeed the conversion of monocytes into macrophages and rapid oxidization of LDL inside the intima take place on a much shorter time scale than the growth of the plaque ([Chalmers et al, 2015](#)). Tracking monocytes within the intima at any given moment would be challenging. Therefore, it is sufficient to view a monocyte as a macrophage and replace LDL with oxLDL. At this point, the plaque is comprised of two separate phases.

One is made up of macrophages and foam cells, while the other includes extracellular matrix, interstitial fluid, oxLDL, cytokines, and more. The initial stage of atherosclerosis can be referred to as the inflammatory cell phase, as it predominantly involves macrophages and foam cells derived from macrophages in the development of the inflammatory disease. Therefore, the second phase is non-inflammatory. Inflammatory cells such as monocytes or macrophages migrate and infiltrate based on the regulation of MCP-1. This chemokine is activated by the endothelial cells and is a key player in the process. The inflammatory cell phase migration is caused by MCP-1 and other cytokines, also known as Endothelial Stimulating cytokines or ES cytokines. These cytokines can be considered as functional cytokines or f-cytokines. The transport of oxLDL and f-cytokines is represented by standard transport reaction equations.

We assume that the domain of the plaque region is  $\Omega(t)$  in  $\mathbb{R}^d$  ( $d = 1, 2, 3$ ) with moving boundary. To begin, we will establish  $\Gamma_1$  as the portion of the plaque boundary related to the interface between the lumen and intima, or the endothelium. Then, we will define  $\Gamma_2(t)$  as the boundary of  $\Omega(t)$  that corresponds to the IEL. This boundary separates the intima from the media and increases in size over time due to the accumulation of macrophages and foam cells. Early plaque formation leads to compensatory expansion of an artery, during which the artery extends radially outward while preserving the lumen (Korshunov et al, 2007). Consequently, the intima-IEL boundary  $\Gamma_2(t)$  can be considered to vary over time. We introduce a finite index set  $\mathcal{C}$  containing the constituents of the plaque region. Based on our assumptions, the plaque is made up of two types of cells: inflammatory cells ( $f$ ) and non-inflammatory cells ( $n$ ), which we can denote as the set  $\mathcal{C} = \{f, n\}$ . Alternatively, we can represent it as  $\mathcal{C} = \{m, f, e\}$ , where  $m$  represents monocyte or macrophage,  $f$  stands for foam cell, and  $e$  denotes extracellular fluid matrix in the plaque region. For this study, we will focus on the two main constituents of the plaque: inflammatory and non-inflammatory cells, i.e.  $\mathcal{C} = \{f, n\}$ . However, it is also possible to consider a multiphase model.

We define  $\varphi^i$  ( $i \in \mathcal{C}$ ) as the volume fraction of each phase and  $\mathbf{v}^i$  ( $i \in \mathcal{C}$ ) as the velocity of each phase. Also, let us denote  $\mathbb{T}^\alpha$  ( $\alpha \in \mathcal{C}$ ) as the stress experienced by the  $\alpha$ -th phase.

## 2.1 Mass Balance Equations

Assume that each phase has the same constant density. Mass balance equations corresponding to each phase can be expressed in the form

$$\frac{\partial \varphi^\alpha}{\partial t} + \nabla \cdot (\varphi^\alpha \mathbf{v}^\alpha) = \mathbb{T}^\alpha, \quad (\alpha \in \mathcal{C}) \quad (1)$$

where  $\mathbf{v}^\alpha \in \mathbb{R}^d$  and  $\mathbb{T}^\alpha \in \mathbb{R}$  is the net source term corresponding to the  $i$ -th phase. Since the plaque is formed by the constituent of  $\mathcal{C}$  and there is no void, thus

$$\sum_{\alpha \in \mathcal{C}} \varphi^\alpha = 1. \quad (2)$$

The plaque growth model suggests that certain cells from our bloodstream, such as monocytes or macrophages, can enter the intima (the innermost layer of our arteries) through damaged parts of the endothelium (the inner lining of our blood vessels). These cells consume oxLDL, which is a type of cholesterol, and then transform into foam cells. Both macrophages and foam cells are involved in the inflammatory phase of plaque growth. Macrophages can accumulate large amounts of oxLDL, which can become toxic to foam cells (Hegy *et al.*, 1996). This toxic environment can also lead to macrophage death, resulting in the cellular debris becoming part of the non-inflammatory phase (Marchant *et al.*, 1996). Assume that there is no local source or sink of material, and mass is transferred between these phases. Inflammatory cells take up material (oxLDL) from the non-inflammatory tissue phase and revert to the non-inflammatory phase upon their death. Therefore, the model is locally mass conservative and consequently satisfies the following:

$$\sum_{\alpha \in \mathcal{C}} \Upsilon^\alpha = 0. \quad (3)$$

## 2.2 Momentum Balance Equations

Under no external force and negligible inertial effect, the momentum balance equations reduce to the balance equations between intraphase and interphase forces for each inflammatory and non-inflammatory phase:

$$\nabla \cdot (\varphi^\alpha \mathbb{T}^\alpha) + \mathbf{I}^{\alpha\beta} = 0, \quad (\alpha \in \mathcal{C}) \quad (4)$$

where  $\mathbb{T}^\alpha \in \mathbb{R}^{d \times d}$  and  $\mathbf{I}^{\alpha\beta} \in \mathbb{R}^d$  is the interphase force exerted on the  $\alpha$ -th phase by the  $\beta$ -th phase. One may note that, according to Newton's third law of motion

$$\sum_{\alpha \in \mathcal{C}} \mathbf{I}^\alpha = 0. \quad (5)$$

In addition, we can simplify the above condition as follows, which is also consistent with the action-reaction principle:

$$\mathbf{I}^{\alpha\beta} = -\mathbf{I}^{\beta\alpha}, \quad \forall \alpha, \beta \in \mathcal{C}, \alpha \neq \beta \quad (6)$$

We assume the interphase force on the  $\alpha$ -th constituent from the Darcy law by the following relations

$$\mathbf{I}^{\alpha\beta} = p \mathbb{I} \nabla \varphi^\alpha + \sum_{\beta \in \mathcal{C}, \beta \neq \alpha} \mathbf{K} \varphi^\alpha \varphi^\beta (\mathbf{v}^\beta - \mathbf{v}^\alpha) \quad (7)$$

in which,  $p \in \mathbb{R}$  is the hydrodynamic pressure of the interstitial fluid. The second term on the right-hand side in equation (7) represents the relative velocity between the phases characterized by a typical drag coefficient  $\mathbf{K} \in \mathbb{R}^{d \times d}$ .

### 2.3 Mass Transport Equations

OxLDL and f-cytokines present within the non-inflammatory phase are governed by the pseudo-steady-state reaction-diffusion equations of the form

$$D_r \nabla \cdot (\varphi^n \nabla c_r) = Q_r, \quad r = \{1, 2\}, \quad (8)$$

in which  $c_1$  and  $c_2$  are concentrations of oxLDL and f-cytokines respectively.  $D_r \in \mathbb{R}$  denotes the diffusion coefficient and  $Q_r \in \mathbb{R}$  represents the net source or sink of the  $r$ -th species. Both  $Q_1$  and  $Q_2$  can be assumed to follow Michaelis-Menten kinetics. The convective transport of the above two species can be neglected without inertia due to the long transport time scale compared to diffusion.

### 2.4 Stress Components

We propose the following constitutive relations corresponding to the stresses  $\mathbb{T}^\alpha$  ( $\alpha = n, f$ ) on the  $\alpha$ -th constituent present in equation (4) (Breward et al, 2003; Watson et al, 2018),

$$\mathbb{T}^f = - (p + \Sigma(\varphi^f) + \Lambda(c_2)) \mathbb{I}, \quad (9)$$

$$\mathbb{T}^n = -p \mathbb{I}, \quad (10)$$

where  $\Sigma : [0, 1] \rightarrow \mathbb{R}$  is a nonlinear function of the volume fraction of the inflammatory phase  $\varphi^f$ ;  $\Lambda : \mathbb{R} \rightarrow \mathbb{R}$  is another nonlinear function of the concentration of the f-cytokines  $c_2$ ;  $\mathbb{I}$  is the identity tensor. To simplify matters, we do not consider viscous forces on either phase, treating these phases as inviscid. As the growth process continues, the increased volume of the foam cells induces a cell-cell interaction. Therefore, beyond a specific value of  $\varphi^f$ , the membrane of each cell starts to deform, and the cells experience stress. In equation (9),  $\Sigma$  on the right-hand side represents the pressure during the inflammatory phase caused by cell-cell interactions. The migration of macrophages from the lumen to the intima is affected by f-cytokines. Therefore, the concentration of f-cytokines, denoted as  $c_2$ , controls the stress in the inflammatory phase. This concentration is expressed by the function  $\Lambda(c_2)$ .

### 2.5 Initial and Boundary conditions

The following initial and boundary conditions are required to complete the model.

#### 2.5.1 Initial Conditions:

Both the inflammatory phase volume fraction and the plaque outer boundary  $\Gamma_2(t)$  are fixed initially:

$$\varphi^f(\mathbf{x}, 0) = \varphi_0^f, \quad \Gamma_2(t = 0) = \Gamma^0, \quad \text{for } \mathbf{x} \in \mathbb{R}^d. \quad (11)$$

#### 2.5.2 Boundary Conditions:

The influx of LDL from the lumen into the intima occurs through the damaged portion of the endothelium. In the presence of free oxygen radicals inside the intima, LDL

molecules oxidize to become oxLDL. The oxidization of LDL takes a much shorter time than plaque growth, as previously assumed. Consequently, both LDL influx and oxidation can be represented as a single process by the oxLDL influx. The flux of oxLDL through  $\Gamma_1$  is assumed to be constant and given by (Chalmers et al, 2015),

$$(\nabla c_1 \cdot \hat{n})|_{\Gamma_1} = -\nu_1. \quad (12)$$

At the boundary  $\Gamma_1$ , the flux of f-cytokines is modelled by

$$(\nabla c_2 \cdot \hat{n})|_{\Gamma_1} = -\nu_2 c_1 + \nu_3 c_2. \quad (13)$$

Chemokines produced at the endothelium in response to oxLDL constitute a family of chemoattractant cytokines that play a significant role in selectively recruiting monocytes etc. (Lusis, 2000). MCP-1, like chemokines produced at the endothelium, recruit monocytes, and the incident is expressed by the first term on the right-hand side of the equation (13). ES cytokines enhance the production of MCP-1. As mentioned earlier, MCP-1, like chemokines and other ES cytokines, is regarded as f-cytokines. Therefore, in this context, it can be said that the production of f-cytokines by the endothelium depends on itself (Chalmers et al, 2015), which justifies the presence of the second term on the right-hand side of equation (13). Consequently, the flux of f-cytokines through the endothelium is influenced by the increasing concentrations of both oxLDL and f-cytokines at the endothelium (Hansson and Libby, 2006). Note that the parameter  $\nu_2$  corresponds to the influx of f-cytokines into the intima, whereas  $\nu_3$  aligns to a modest outflux from the intima through the endothelium. This assumption is considered reasonable in the given context by following the framework presented in Chalmers et al (2015).

On the moving plaque boundary  $\Gamma_2(t)$ , we assume continuity of stress so that total stress of inflammatory and non-inflammatory cell phase is same as the stress of the outer region which is supposed to be constant. We set

$$(\mathbb{T}^f + \mathbb{T}^n)|_{\Gamma_2(t)} = \mathbb{T}^\infty. \quad (14)$$

We also assume that outside the plaque boundary  $\Gamma_2(t)$ , oxLDL and f-cytokines concentration are constant, and thus we set

$$c_1|_{\Gamma_2(t)} = c_1^\infty, \quad (15)$$

$$c_2|_{\Gamma_2(t)} = c_2^\infty. \quad (16)$$

Finally, we assume that the plaque moving boundary  $\Gamma_2(t)$  expands at the same speed as the inflammatory cells on the boundary. Therefore, we define the following:

$$\frac{d\Gamma_2}{dt} = \mathbf{v}^f|_{\Gamma_2(t)}. \quad (17)$$

## 2.6 Constitutive Assumptions

### 2.6.1 Inflammatory Cell Phase Source Term

Macrophages migrate into the intima in response to f-cytokines. Experimental studies support the notion that f-cytokines, particularly MCP-1, stimulate macrophage proliferation during the progression of plaque formation (Zheng et al, 2016). Foam cells are produced when macrophages consume oxLDL, present in the non-inflammatory phase. Therefore, the production of inflammatory cells depends on the concentration of oxLDL ( $c_1$ ) and f-cytokines ( $c_2$ ). On the other hand, the primary cause of inflammatory cell death is oxLDL-induced toxicity due to the excess concentration of  $c_1$ . Therefore, we choose  $\Upsilon_f$  by assuming both production and degradation or death saturating rates following Michaelis-Menten kinetics:

$$\Upsilon_f = \underbrace{\varphi^f \varphi^n \left( \frac{s_0 c_2}{1 + s_1 c_2} + \frac{s_2 c_1}{1 + s_3 c_1} \right)}_{\text{production}} - \underbrace{\varphi^f \left( \frac{s_4 + s_5 c_1}{1 + s_6 c_1} \right)}_{\text{death}} \mathcal{H}(c_1 - c_1^*), \quad (18)$$

where the first two terms correspond to the production of inflammatory cells characterized by the parameters  $s_0$ ,  $s_1$ ,  $s_2$ , and  $s_3$ , and the second term represents the death of inflammatory cells characterized by  $s_4$ ,  $s_5$ , and  $s_6$ . The production rate of inflammatory cells increases with  $c_1$  up to a fixed value  $c_1^*$  (can be referred to as oxLDL-induced reference toxicity level), beyond which oxLDL results in the death of inflammatory cells. In other words, beyond such  $c_1^*$ , the death rate of inflammatory cells increases with  $c_1$ .  $\mathcal{H}$  in equation (18) denotes the Heaviside function which can be approximated by a smooth function as (Hubbard and Byrne, 2013)

$$\mathcal{H}(x, \epsilon) = \frac{1}{2} \left\{ 1 + \tanh \left( \frac{x}{\epsilon} \right) \right\}, \quad \epsilon \ll 1. \quad (19)$$

### 2.6.2 OxLDL and f-Cytokines Source Terms

Net source or sink of oxLDL  $Q_1$  can be assumed as follows

$$Q_1 = \underbrace{\varphi^f \varphi^n \left( \frac{q_0 c_1}{1 + q_1 c_1} \right)}_{\text{consumption}} - \underbrace{\varphi^f \varphi^n (q_2 c_1)}_{\text{release}}, \quad (20)$$

in which  $q_0$ ,  $q_1$  and  $q_2$  are positive constants. The first term on the right side describes the loss of oxLDL due to the oxLDL consumption by macrophages to become foam cells. We use a Michaelis-Menten general kinetics type function to represent it. The oxLDL released by the dead foam cells are assumed to obey a constant decay rate (see the second term on the right-hand side of equation (20)) (Berliner et al, 1995). Note that there may be a loss of oxLDL, perhaps through degradation, but we do not include this for simplicity.

Similarly,  $Q_2$  can be set as

$$Q_2 = \underbrace{\varphi^n q_3 c_2}_{\text{decay}} - \underbrace{\varphi^n \varphi^f (q_4 c_1 c_2)}_{\text{production}}, \quad (21)$$

where  $q_3$  and  $q_4$  are positive constants. Cytokines secreted from foam cells in presence of oxLDL (Chalmers et al, 2017). Correspondingly, the production of f-cytokines depends on  $\varphi^f$  and  $c_1$ , as shown by the second term of the right hand side of above equation. The first term represents a linear decay in  $c_2$ .

### 2.6.3 Terms Contributing on Stress Tensor

The function  $\Sigma$  in equation (9) represents the pressure on inflammatory cell phase due to cell-cell interactions, which can be expressed as

$$\Sigma(\varphi^f) = \frac{(\varphi^f - \varphi^*)}{(1 - \varphi^f)^2} \mathcal{H}(\varphi^f - \varphi^*), \quad (22)$$

where  $\varphi^*$  is the volume fraction of foam cells and macrophages beyond which cells experience stress. Our choice of  $\Sigma$  follows the study of Breward et al (2002); Byrne et al (2003), etc. f-Cytokines act as chemoattractants to pull monocytes from the lumen into the intima. It has already been mentioned that monocytes rapidly transform into macrophages inside the intima. Hence, the movement of macrophages within the intima can be assumed to be influenced by f-cytokines concentration (i.e. chemotaxis). Therefore,  $\Lambda$  in equation (9) can be defined to be

$$\Lambda = \frac{\chi}{1 + (\kappa c_2)^m}, \quad (23)$$

where  $\chi$ ,  $\kappa$  and  $m$  are positive parameters. The assumption implies that the stress from the inflammatory phase decreases with increasing f-cytokines concentration, allowing the chemoattractant to move. Correspondingly, it is represented as a mechanism of stress relief in the inflammatory cell phase (Watson et al, 2018). The chemotactic function  $\Lambda$  also can be defined as  $\chi/(1 + \kappa c_2)^2$ , but in the case of the receptor binding, it may be more reasonable to describe by Hill function as shown in (23) (Hillen and Painter, 2009). In this model, monocytes enter the intima from the bloodstream with the help of receptors VCAM-1 and ICAM-1. Consequently, our study would prefer to consider the chemotaxis function as (23).

## 3 1D Model

As the first step, we study plaque growth in one dimension along the  $x$ -axis. It occupies the region  $0 \leq x \leq l(t)$  (see Fig. 2). Consequently, the boundary  $\Gamma_1$  reduces to  $x = 0$  (i.e., the interface of the endothelium and intima), and the moving edge  $\Gamma_2(t)$  corresponds to the interface of the intima. IEL is now  $x = l(t)$ , which is the width of the growing plaque at time  $t$  in the early stage. This one-dimensional model would

enable us to focus on the cellular and biochemical mechanisms without worrying about the geometry of the domain. Furthermore, the diameter of an artery is significantly larger than the width of the intima at the early stages of plaque formation (Bonithon-Kopp et al, 1996), which makes it reasonable to use Cartesian coordinates as an approximation for radial coordinates. We denote all the physical variables consistent with the previous section. The above scenario compels us to reduce the mass balance equations (1) into the following form:

$$\frac{\partial \varphi^f}{\partial t} + \frac{\partial}{\partial x} (\varphi^f v^f) = \Upsilon^f, \quad (24)$$

$$\frac{\partial \varphi^n}{\partial t} + \frac{\partial}{\partial x} (\varphi^n v^n) = \Upsilon^n. \quad (25)$$

Similarly, the momentum conservation equations (4) reduce as,

$$\frac{\partial}{\partial x} (\varphi^f T^f) + I^{fn} = 0, \quad (26)$$

$$\frac{\partial}{\partial x} (\varphi^n T^n) + I^{nf} = 0, \quad (27)$$

in which

$$I^{fn} = p \frac{\partial \varphi^f}{\partial x} + k \varphi^f \varphi^n (v^n - v^f) \quad (28)$$

and

$$I^{nf} = p \frac{\partial \varphi^n}{\partial x} + k \varphi^f \varphi^n (v^f - v^n), \quad (29)$$

as obtained from (7). The stresses described in equations (9) and (10) are reduced to the following 1D form

$$T^f = -(p + \Sigma(\varphi^f) + \Lambda(c_2)) \quad (30)$$

and

$$T^n = -p \quad (31)$$

respectively.

Next, the mass transport equations (8) reduce to

$$D_1 \frac{\partial}{\partial x} \left( \varphi^n \frac{\partial c_1}{\partial x} \right) = Q_1, \quad (32)$$

$$D_2 \frac{\partial}{\partial x} \left( \varphi^n \frac{\partial c_2}{\partial x} \right) = Q_2. \quad (33)$$

Finally, The initial and boundary conditions (11)-(17) become

$$\varphi^f = \varphi_0^f, \quad l = l_0, \quad \text{at } t = 0, \quad (34)$$

$$D_1 \left( \frac{\partial c_1}{\partial x} \right) = -\nu_1, \quad \text{at } x = 0, \quad (35)$$

$$D_2 \left( \frac{\partial c_2}{\partial x} \right) = -\nu_2 c_1 + \nu_3 c_2, \quad \text{at } x = 0, \quad (36)$$

$$T^f + T^n = T^\infty, \quad \text{at } x = l(t), \quad (37)$$

$$c_1 = c_1^\infty, \quad \text{at } x = l(t), \quad (38)$$

$$c_2 = c_2^\infty, \quad \text{at } x = l(t), \quad (39)$$

and

$$\frac{dl}{dt} = v^f. \quad \text{at } x = l(t). \quad (40)$$

## 4 Model Simplification

The entire model of early stage plaque growth is expressed into a system of nonlinear partial differential equations in  $\varphi^f$ ,  $v^f$ ,  $c_1$  and  $c_2$ . The simplification of this model follows the similar approach to that of [Breward et al \(2002\)](#); [Byrne and Preziosi \(2003\)](#); [Watson et al \(2018\)](#), and for clarity, the model simplification is included in detail. First we add the mass balance equations (24) and (25), to get

$$\frac{\partial}{\partial x} (\varphi^f v^f + \varphi^n v^n) = 0, \quad (41)$$

which upon integration results

$$(\varphi^f v^f + \varphi^n v^n) = v_0^{\text{com}}, \quad (42)$$

where the right hand side of the above equation stands for the composite velocity of the mixture at the endothelium-intima interface (EII). It is reasonable to impose  $v^n(0) = 0$  within  $v_0^{\text{com}}$  as the non-inflammatory phase cannot escape from the plaque. Hence,  $v_0^{\text{com}}$  becomes the product of inflammatory cell phase volume fraction and corresponding velocity at  $x = 0$ , which will be denoted as  $V_0$ . Consequently,  $v^n$  is expressed as follows

$$v^n = \left( \frac{V_0 - \varphi^f v^f}{\varphi^n} \right). \quad (43)$$

Apparently,  $V_0$  becomes the velocity of macrophages at  $x = 0$  with which they enter the intima under the influence of f-cytokines. Realistic value of  $V_0$  can be obtained from literature (According to [van den Bos et al \(2020\)](#),  $V_0$  is of order  $1 \mu\text{m}/\text{min}$ ).

Now, summing the momentum balance equations (26) and (27), and submitting the stress expressions  $T^f$  and  $T^n$  from (30)-(31), we obtain

$$\frac{\partial p}{\partial x} + \frac{\partial F}{\partial x} = 0, \quad (44)$$

where

$$F = \varphi^f (\Sigma + \Lambda). \quad (45)$$

We derive the following from (44) with the help of (26), (28) and (30):

$$\varphi^n \frac{\partial F}{\partial x} + k (\varphi^f v^f - \varphi^f V_0) = 0. \quad (46)$$

Consequently, with the help of mass balance equation (24), we deduce

$$\frac{\partial \varphi^f}{\partial t} + V_0 \frac{\partial \varphi^f}{\partial x} - \frac{\varphi^n}{k} \left[ \frac{\partial^2 F}{\partial x^2} + \frac{1}{\varphi^n} \frac{\partial \varphi^n}{\partial x} \frac{\partial F}{\partial x} \right] = \Upsilon^f. \quad (47)$$

Now, from the equations (46) and (43) and employing the expression of  $F$  as provided in equation (45), we derive the following:

$$k (v^n - V_0) = \frac{\partial}{\partial x} (\varphi^f \Lambda) + \frac{\partial}{\partial x} (\varphi^f \Sigma). \quad (48)$$

Using the condition,  $v^n = 0$  at  $x = 0$ , we arrive at the following boundary condition

$$\frac{\partial}{\partial x} (\varphi^f \Lambda) + \frac{\partial}{\partial x} (\varphi^f \Sigma) + k V_0 = 0 \quad \text{at } x = 0, \quad (49)$$

which suggests the influx of inflammatory cells inside the intima via a chemotactic response to the f-cytokines at the endothelium-intima interface (EII).

Furthermore, from the stress boundary condition equation (61), at  $x = l(t)$  we have

$$T^f + T^n = 1, \quad (50)$$

which further reduces to at  $x = l(t)$ :

$$\Sigma(\varphi^f) + \Lambda(c_2) + (2p + 1) = 0. \quad (51)$$

At the plaque boundary  $x = l(t)$ , we assume the interstitial hydrodynamic pressure ( $p$ ) in such a way that  $2p + 1 = 0$ . We therefore have

$$\Sigma(\varphi^f) + \Lambda(c_2) = 0, \quad \text{at } x = l(t). \quad (52)$$

Therefore, our reduced model can be read as the equation (47) coupled with equations (46), (32) and (33) subject to the initial and boundary conditions prescribed by (34)-(36), (38)-(40), (49) and (52).

#### 4.1 Nondimensionalization

Using hat ( $\hat{\cdot}$ ) to denote dimensionless quantities, we scale the independent and dependent variables  $x, t, l, v^f, c_1, c_2, \varphi^f$  and  $\varphi^n$ , as follows (one can note that, inflammatory and non-inflammatory cell phase volume fractions  $\varphi^f$  and  $\varphi^n$  respectively do

not require scaling):

$$\hat{x} = x/l_0, \quad \hat{t} = t/(kl_0^2/T^\infty), \quad \hat{l} = l/l_0, \quad \hat{v}^f = v^f/(T^\infty/kl_0).$$

$$\hat{c}_1 = c_1/c_1^\infty, \quad \hat{c}_2 = c_2/c_2^\infty, \quad \hat{\varphi}^f = \varphi^f, \quad \hat{\varphi}^n = \varphi^n.$$

We introduced the non-dimensional parameters in the following way:

$$\hat{\Upsilon}^f = \Upsilon^f/(T^\infty/kl_0^2), \quad \hat{\Sigma} = \Sigma/T^\infty, \quad \hat{\Lambda} = \Lambda/T^\infty, \quad \hat{T}^f = T^f/T^\infty,$$

$$\hat{T}^n = T^n/T^\infty, \quad \hat{F} = F/T^\infty, \quad \hat{Q}_1 = Q_1/(D_1c_1^\infty/l_0^2), \quad \hat{Q}_2 = Q_2/(D_2c_2^\infty/l_0^2),$$

$$\hat{\nu}_1 = \nu_1/(D_1c_1^\infty/l_0), \quad \hat{\nu}_2 = \nu_2/(D_2c_2^\infty/l_0c_1^\infty), \quad \hat{\nu}_3 = \nu_3/(1/l_0), \quad \hat{V}_0 = V_0/(T^\infty/kl_0).$$

The corresponding model equations, initial and boundary conditions in non-dimensional form reduces to

$$\frac{\partial \hat{\varphi}^f}{\partial \hat{t}} + \hat{V}_0 \frac{\partial \hat{\varphi}^f}{\partial \hat{x}} - \hat{\varphi}^n \frac{\partial^2 \hat{F}}{\partial \hat{x}^2} - \frac{\partial \hat{\varphi}^n}{\partial \hat{x}} \frac{\partial \hat{F}}{\partial \hat{x}} = \hat{\Upsilon}^f \quad (53)$$

$$\hat{\varphi}^n \frac{\partial \hat{F}}{\partial \hat{x}} + \hat{\varphi}^f (\hat{v}^f - \hat{V}_0) = 0, \quad (54)$$

$$\frac{\partial}{\partial \hat{x}} \left( \hat{\varphi}^n \frac{\partial \hat{c}_1}{\partial \hat{x}} \right) = \hat{Q}_1, \quad (55)$$

$$\frac{\partial}{\partial \hat{x}} \left( \hat{\varphi}^n \frac{\partial \hat{c}_2}{\partial \hat{x}} \right) = \hat{Q}_2, \quad (56)$$

$$\hat{\varphi}^f = \varphi_0^f, \quad \hat{l} = 1, \quad \text{at } \hat{t} = 0, \quad (57)$$

$$\frac{\partial}{\partial \hat{x}} \left( \hat{\varphi}^f \hat{\Lambda} + \hat{\varphi}^f \hat{\Sigma} \right) + \hat{V}_0 = 0, \quad \text{at } \hat{x} = 0, \quad (58)$$

$$\frac{\partial \hat{c}_1}{\partial \hat{x}} = -\hat{\nu}_1, \quad \text{at } \hat{x} = 0, \quad (59)$$

$$\frac{\partial \hat{c}_2}{\partial \hat{x}} = -\hat{\nu}_2 \hat{c}_1 + \hat{\nu}_3 \hat{c}_2, \quad \text{at } \hat{x} = 0, \quad (60)$$

$$\hat{\Sigma}(\hat{\varphi}^f) + \hat{\Lambda}(\hat{c}_2) = 0, \quad \text{at } \hat{x} = \hat{l}(t), \quad (61)$$

$$\hat{c}_1 = 1, \quad \text{at } \hat{x} = \hat{l}(t), \quad (62)$$

$$\hat{c}_2 = 1, \quad \text{at } \hat{x} = \hat{l}(t), \quad (63)$$

and

$$\frac{d\hat{l}}{d\hat{t}} = \hat{v}^f. \quad \text{at } \hat{x} = \hat{l}(t). \quad (64)$$

Without loss of generality, we drop the hat ('^') from the model field equations, and initial and boundary conditions unless otherwise stated explicitly.

## 4.2 Change of Variables

In order to execute numerical solutions, it is convenient to map the moving domain onto a fixed one. Consequently, we change the variable  $(x, t)$  to  $(\zeta, \tau)$  by the transformation  $\zeta = x/l(t)$  and  $\tau = t$ . The transformed problem reduces to

$$\frac{\partial \varphi^f}{\partial \tau} - \left( \zeta \frac{dl}{d\tau} - \frac{V_0}{l} \right) \frac{\partial \varphi^f}{\partial \zeta} - \frac{\varphi^n}{l^2} \frac{\partial^2 F}{\partial \zeta^2} - \frac{1}{l^2} \frac{\partial \varphi^n}{\partial \zeta} \frac{\partial F}{\partial \zeta} = \Upsilon^f, \quad (65)$$

$$\varphi^n \frac{\partial F}{\partial \zeta} + l \varphi^f (v^f - V_0) = 0, \quad (66)$$

$$\frac{\partial}{\partial \zeta} \left( \varphi^n \frac{\partial c_1}{\partial \zeta} \right) = l^2 Q_1, \quad (67)$$

$$\frac{\partial}{\partial \zeta} \left( \varphi^n \frac{\partial c_2}{\partial \zeta} \right) = l^2 Q_2, \quad (68)$$

with initial and boundary conditions

$$\varphi^f = \varphi_0^f, \quad l = 1, \quad \text{at } \tau = 0 \quad (69)$$

$$\frac{\partial}{\partial \zeta} (\varphi^f \Lambda) + \frac{\partial}{\partial \zeta} (\varphi^f \Sigma) + l V_0 = 0, \quad \text{at } \zeta = 0, \quad (70)$$

$$\frac{\partial c_1}{\partial \zeta} = -l \nu_1, \quad \text{at } \zeta = 0, \quad (71)$$

$$\frac{\partial c_2}{\partial \zeta} = -l \nu_2 c_1 + l \nu_3 c_2, \quad \text{at } \zeta = 0, \quad (72)$$

$$\Sigma(\varphi^f) + \Lambda(c_2) = 0, \quad \text{at } \zeta = 1, \quad (73)$$

$$c_1 = 1, \quad \text{at } \zeta = 1, \quad (74)$$

$$c_2 = 1, \quad \text{at } \zeta = 1, \quad (75)$$

and

$$\frac{dl}{d\tau} = v^f \quad \text{at } \zeta = 1. \quad (76)$$

## 5 Computational Technique

A stable finite difference scheme for the numerical solution of the governing equations is employed. Specifically, explicit finite difference methods are applied to solve parabolic-type partial differential equations. The present differential nonlinear system is parabolic and amenable to using explicit finite-difference formulation. To solve the problem, we utilized the explicit finite-difference scheme known as the forward-time central space (FTCS) method, following the approach outlined in the studies by [Zaman et al \(2016\)](#); [Lee et al \(2013\)](#). One can refer to the book by [Hoffmann and Chiang \(2000\)](#) for comprehensive details of the method. This scheme approximates spatial derivatives by central difference formulae, while the forward difference formula approximates the time derivative.

We discretize the region  $(0,1)$  into  $N$  equal cells of size  $\Delta\zeta = 1/N + 1$  with a time step  $\Delta\tau > 0$ . Define  $\zeta_j = (j-1)\Delta\zeta$ ,  $j = 1, 2, \dots, N+1$ , and  $\tau_n = (n-1)\Delta\tau$ ,  $n = 1, 2, \dots$ , and approximations  $[\varphi^f]_j^n = \varphi^f(\zeta_j, \tau_n)$ ,  $[c_1]_j^n = c_1(\zeta_j, \tau_n)$ , and  $[c_2]_j^n = c_2(\zeta_j, \tau_n)$ . Spatial and time derivative approximations are as follows:

$$\frac{\partial c_\ell}{\partial \zeta} \cong \frac{[c_\ell]_{j+1}^n - [c_\ell]_{j-1}^n}{2\Delta\zeta}, \quad \ell = 1, 2 \quad (77)$$

$$\frac{\partial^2 c_\ell}{\partial \zeta^2} \cong \frac{[c_\ell]_{j+1}^n - 2[c_\ell]_j^n + [c_\ell]_{j-1}^n}{(\Delta\zeta)^2}, \quad \ell = 1, 2 \quad (78)$$

$$\frac{\partial \varphi^f}{\partial \zeta} \cong \frac{[\varphi^f]_{j+1}^n - [\varphi^f]_{j-1}^n}{2\Delta\zeta}, \quad (79)$$

$$\frac{\partial^2 \varphi^f}{\partial \zeta^2} \cong \frac{[\varphi^f]_{j+1}^n - 2[\varphi^f]_j^n + [\varphi^f]_{j-1}^n}{(\Delta\zeta)^2}, \quad (80)$$

and

$$\frac{\partial \varphi^f}{\partial \tau} \cong \frac{[\varphi^f]_j^{n+1} - [\varphi^f]_j^n}{\Delta\tau}. \quad (81)$$

The system (65)-(76) is discretized based on the approximations (77)-(81) and solved. We start with a given  $[\varphi^f]_j^n$  to compute  $[c_1]_j^n$ ,  $[c_2]_j^n$  using which  $[\varphi^f]_j^{n+1}$  is evaluated. To meet the CFL condition of the explicit scheme and achieve an accuracy of approximately  $10^{-7}$ , we took  $N = 30$  spatial steps and  $10^5$  time steps, ensuring the stability of the corresponding method through the CFL condition.

In equation (67), the term  $Q_1$  is nonlinear in  $c_1$ . Applying the central difference formula (77)-(78) in (67), a system of nonlinear equations in  $[c_1]_1^n, [c_1]_2^n, \dots, [c_1]_{N+1}^n$  when  $q_1 \neq 0$  is obtained. Newton's method can solve this nonlinear system, which is a tedious job requiring high numerical programming skills. As a result, some studies assume  $q_1 = 0$  to remove the nonlinearity (Breward et al, 2002; Lee et al, 2013). But, this restricts the general kinetics and reduces it to first-order kinetics, a particular case of Michaelis–Menten kinetics. In the present study, we deal with the general kinetics and consider  $q_1$  as a small parameter ( $q_1 \ll 1$ ) so that it becomes a perturbation parameter rather than taking the vanishing limit. Therefore, we reduce the nonlinear form of  $Q_1$  in the variable  $c_1$  to a weakly linearized form using perturbation approximation with the perturbed parameter  $q_1$  as described in the following section.

## 5.1 Perturbation Approximations

We consider the following perturbation approximations

$$c_\ell = c_\ell^{(0)} + q_1 c_\ell^{(1)} + \mathcal{O}(q_1^2), \quad \ell = 1, 2 \quad (82)$$

$$\varphi^f = (\varphi^f)^{(0)} + q_1 (\varphi^f)^{(1)} + \mathcal{O}(q_1^2), \quad (83)$$

$$v^f = (v^f)^{(0)} + q_1 (v^f)^{(1)} + \mathcal{O}(q_1^2). \quad (84)$$

Using the above approximations, we can get the following expansions

$$\varphi^n = (\varphi^n)^{(0)} + q_1(\varphi^n)^{(1)} + \mathcal{O}(q_1^2), \quad (85)$$

$$\Upsilon^f = \Upsilon^f{}^{(0)} + q_1\Upsilon^f{}^{(1)} + \mathcal{O}(q_1^2), \quad (86)$$

$$\Sigma = \Sigma^{(0)} + q_1\Sigma^{(1)} + \mathcal{O}(q_1^2), \quad (87)$$

$$\Lambda = \Lambda^{(0)} + q_1\Lambda^{(1)} + \mathcal{O}(q_1^2), \quad (88)$$

$$F = F^{(0)} + q_1F^{(1)} + \mathcal{O}(q_1^2), \quad (89)$$

and

$$Q_\ell = Q_\ell^{(0)} + q_1Q_\ell^{(1)} + \mathcal{O}(q_1^2), \quad \ell = 1, 2 \quad (90)$$

where the expressions of  $(\varphi^n)^{(0)}$ ,  $(\varphi^n)^{(1)}$ ,  $\Upsilon^f{}^{(0)}$ ,  $\Upsilon^f{}^{(1)}$ ,  $\Sigma^{(0)}$ ,  $\Sigma^{(1)}$ ,  $\Lambda^{(0)}$ ,  $\Lambda^{(1)}$ ,  $F^{(0)}$ ,  $F^{(1)}$ ,  $Q_1^{(0)}$ ,  $Q_1^{(1)}$ ,  $Q_2^{(0)}$ , and  $Q_2^{(1)}$  are described in the Appendix A and B. Correspondingly, the leading and  $\mathcal{O}(q_1)$  problems reduce as shown in the following sections.

### 5.1.1 The Leading Order Problem

The governing equations and the initial and boundary conditions corresponding to the leading order problem reduce as shown in Table 1.

### 5.1.2 The $\mathcal{O}(q_1)$ Problem

In the first order, the governing equations and the initial and boundary conditions reduce as shown in Table 2.

Now, the terms  $Q_1^{(0)}$  and  $Q_1^{(1)}$  are both linear in  $c_1^{(0)}$  and  $c_1^{(1)}$  respectively (see Appendix A & B). Therefore, in order to compute  $c_1^{(0)}$  and  $c_1^{(1)}$  numerically from the equations in Table 1 and 2 (specifically, the third governing equations from both tables), we can apply central difference formulae (77)-(78). Correspondingly, we will get a system of linear equations for each case which can be solved using the Thomas algorithm. Then we compute  $c_2^{(0)}$ ,  $c_2^{(1)}$  in a similar way and finally we evaluate  $(\varphi^n)^{(0)}$  and  $(\varphi^n)^{(1)}$ . Consequently, we numerically obtain the solution of the leading and  $\mathcal{O}(q_1)$  problem. Hence, the complete solution is determined upto  $\mathcal{O}(q_1)$  from the equations (82)-(84).

## 6 Numerical Simulations

In this section, we systematically analyze the numerical results on the oxidized LDL concentration, volume of inflammatory phase (foam cells + macrophages), concentration of f-cytokines responsible for macrophage migration, the variation of plaque width over time, etc. First, we set the values of parameters of interest. Subsequently, numerical simulations are performed.

**Table 1:** Governing equations, along with initial and boundary conditions related to the leading order problem.

<u>Governing Equations</u>
$\frac{\partial(\varphi^f)^{(0)}}{\partial\tau} - \left(\frac{\zeta}{l} \frac{dl}{d\tau} - \frac{V_0}{l}\right) \frac{\partial(\varphi^f)^{(0)}}{\partial\zeta} - \frac{(\varphi^f)^{(0)}}{l^2} \frac{\partial^2 F^{(0)}}{\partial\zeta^2} - \frac{1}{l^2} \frac{\partial(\varphi^n)^{(0)}}{\partial\zeta} \frac{\partial F^{(0)}}{\partial\zeta} = \Upsilon^f{}^{(0)},$
$(\varphi^n)^{(0)} \frac{\partial F^{(0)}}{\partial\zeta} + l(\varphi^f)^{(0)} (v^f)^{(0)} = lV_0,$
$\frac{\partial}{\partial\zeta} \left( (\varphi^n)^{(0)} \frac{\partial c_1^{(0)}}{\partial\zeta} \right) = l^2 Q_1^{(0)},$
$\frac{\partial}{\partial\zeta} \left( (\varphi^n)^{(0)} \frac{\partial c_2^{(0)}}{\partial\zeta} \right) = l^2 Q_2^{(0)},$
<u>Initial Conditions</u>
$(\varphi^f)^{(0)} = \varphi_0^f, \quad l = 1, \quad \text{at } \tau = 0,$
<u>Boundary Conditions</u>
$\frac{\partial}{\partial\zeta} \left[ (\varphi^f)^{(0)} (\Lambda^{(0)} + \Sigma^{(0)}) \right] = 0, \quad \text{at } \zeta = 0,$
$\frac{\partial c_1^{(0)}}{\partial\zeta} = -l\nu_1, \quad \text{at } \zeta = 0,$
$\frac{\partial c_2^{(0)}}{\partial\zeta} = -l\nu_2 c_1^{(0)} + l\nu_3 c_2^{(0)}, \quad \text{at } \zeta = 0,$
$\Sigma^{(0)} \left( (\varphi^f)^{(0)} \right) + \Lambda^{(0)} \left( c_2^{(0)} \right) = 0, \quad \text{at } \zeta = 1,$
$c_1^{(0)} = 1, \quad \text{at } \zeta = 1,$
$c_2^{(0)} = 1, \quad \text{at } \zeta = 1,$
$\frac{dl}{d\tau} = (v^f)^{(0)} \quad \text{at } \zeta = 1.$

## 6.1 Model Parameterisations

The development of plaque in atherosclerosis occurs gradually over time. Therefore, the time scale for the simulation is considered in days. According to Hao et al. (2014), Hao and Friedman (2014), the diffusion coefficients for oxidized LDL and f-cytokines (in particular for MCP-1) are  $29.89 \text{ cm}^2\text{day}^{-1}$  and  $17.28 \text{ cm}^2\text{day}^{-1}$  respectively.  $q_0$  represents the rate of metabolism of oxidized LDL by macrophages, which is  $10^4$

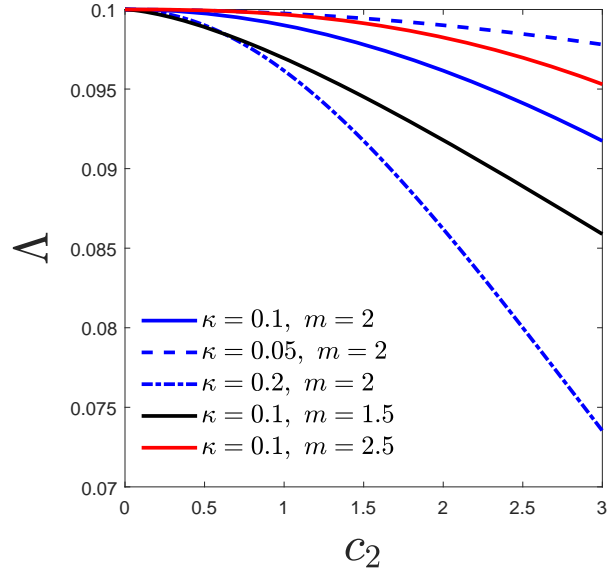
**Table 2:** Governing equations, along with initial and boundary conditions corresponding to the  $\mathcal{O}(q_1)$  problem.

---

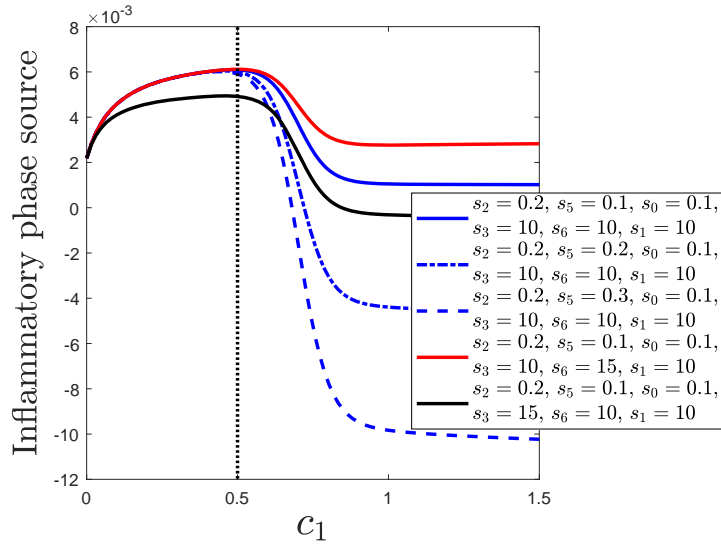
<b>Governing Equations</b>
$\frac{\partial(\varphi^f)^{(1)}}{\partial\tau} - \left(\frac{\zeta}{l} \frac{dl}{d\tau} - \frac{V_0}{l}\right) \frac{\partial(\varphi^f)^{(1)}}{\partial\zeta} - \frac{(\varphi^n)^{(0)}}{l^2} \frac{\partial^2 F^{(1)}}{\partial\zeta^2} - \frac{(\varphi^n)^{(1)}}{l^2} \frac{\partial^2 F^{(0)}}{\partial\zeta^2} - \frac{1}{l^2} \frac{\partial(\varphi^n)^{(0)}}{\partial\zeta} \frac{\partial F^{(1)}}{\partial\zeta} - \frac{1}{l^2} \frac{\partial(\varphi^n)^{(1)}}{\partial\zeta} \frac{\partial F^{(0)}}{\partial\zeta} = \Upsilon^f{}^{(1)},$ $(\varphi^n)^{(0)} \frac{\partial F^{(1)}}{\partial\zeta} + (\varphi^n)^{(1)} \frac{\partial F^{(0)}}{\partial\zeta} + l(\varphi^f)^{(0)} (v^f)^{(1)} + l(\varphi^f)^{(1)} \left( (v^f)^{(0)} - V_0 \right) = 0,$ $\frac{\partial}{\partial\zeta} \left( (\varphi^n)^{(0)} \frac{\partial c_1^{(1)}}{\partial\zeta} + (\varphi^n)^{(1)} \frac{\partial c_1^{(0)}}{\partial\zeta} \right) = l^2 Q_1^{(1)},$ $\frac{\partial}{\partial\zeta} \left( (\varphi^n)^{(0)} \frac{\partial c_2^{(1)}}{\partial\zeta} + (\varphi^n)^{(1)} \frac{\partial c_2^{(0)}}{\partial\zeta} \right) = l^2 Q_2^{(1)},$
<b>Initial Conditions</b>
$(\varphi^f)^{(1)} = 0, \quad l = 1, \quad \text{at } \tau = 0,$
<b>Boundary Conditions</b>
$\frac{\partial}{\partial\zeta} \left( (\varphi^f)^{(0)} \Lambda^{(1)} + (\varphi^f)^{(1)} \Lambda^{(0)} \right) + \frac{\partial}{\partial\zeta} \left( (\varphi^f)^{(0)} \Sigma^{(1)} + (\varphi^f)^{(1)} \Sigma^{(0)} \right) = 0, \quad \text{at } \zeta = 0,$ $\frac{\partial c_1^{(1)}}{\partial\zeta} = 0, \quad \text{at } \zeta = 0,$ $\frac{\partial c_2^{(1)}}{\partial\zeta} = -l\nu_2 c_1^{(1)} + l\nu_3 c_2^{(1)}, \quad \text{at } \zeta = 0,$ $\Sigma^{(1)} + \Lambda^{(1)} = 0, \quad \text{at } \zeta = 1,$ $c_1^{(1)} = 0, \quad \text{at } \zeta = 1,$ $c_2^{(1)} = 0. \quad \text{at } \zeta = 1.$

---

day<sup>-1</sup> (McKay et al, 2005). Similarly, the study of Cobbold et al (2002) suggests the value of  $q_2$  (the rate of oxLDL production) as  $2.35 \times 10^{-7}$  day<sup>-1</sup>. In addition, Hao and Friedman (2014) and Chen et al (2012) respectively support the production and decay rates of f-cytokines (i.e.,  $q_4$  and  $q_3$ ) as  $0.96 \times 10^{10}$  g<sup>-1</sup>cm<sup>3</sup>day<sup>-1</sup> and 1.73 day<sup>-1</sup>. As reported by Hao and Friedman (2014), within the intima, the concentration of oxLDL and f-cytokines are  $7 \times 10^{-4} - 1.9 \times 10^{-3}$  gcm<sup>-3</sup> and  $3 \times 10^{-10}$  gcm<sup>-3</sup> respectively. The chemotactic sensitivity parameter  $\chi$ , as mentioned in equation (23) can be set as  $15.5 \times 10^{-16}$  gcm<sup>-1</sup>day<sup>-2</sup> (Kim and Friedman, 2010). Further, the



(a)



(b)

**Fig. 3:** Variation of (a) chemotactic function  $\Lambda$  with respect to  $c_2$ , (b) inflammatory phase source  $\Upsilon^f$  with  $c_1$  corresponding to various parameters described in the figures.

clinical study of [Grootaert et al \(2015\)](#) mentions a standard intimal width as  $75\mu\text{m}$ .

Since the early plaque growth is restricted within the intima, one can choose the initial plaque width as  $10^{-2}$  cm. With the data set mentioned above, we calculate the corresponding non-dimensional values of the parameters  $q_0, q_2, q_3, q_4$  and  $\chi$  as listed in Table 3. In addition, this table contains the calculated dimensionless values of constants  $\nu_1, \nu_2$  and  $\nu_3$  that are present in equations (71)-(72) from the studies of Chalmers et al (2015); Ougrinovskaia et al (2010).

**Table 3:** Calculated dimensionless values of the parameters from the mentioned literatures.

Parameter	Dimensionless value	Supporting literature
$q_0$	$3.3 \times 10^{-1}$	McKay et al (2005)
$q_2$	$7.8 \times 10^{-14}$	Cobbold et al (2002)
$q_3$	$1 \times 10^{-6}$	Chen et al (2012)
$q_4$	$5 \times 10^{-1}$	Hao and Friedman (2014)
$\chi$	$1 \times 10^{-1}$	Kim and Friedman (2010)
$\kappa$	$1 \times 10^{-1}$	—
$m$	2	—
$l_0$	$10^{-2}$	Grootaert et al (2015)
$V_0$	$10^{-3}$	van den Bos et al (2020)
$\nu_1$	$10^{-2} - 10^1$	Chalmers et al (2015)
$\nu_2$	$10^{-2} - 10^1$	Ougrinovskaia et al (2010)
$\nu_3$	$10^{-3} - 10^1$	Chalmers et al (2015)

It has been noted that there is a need for more literature to accurately determine the values of the non-dimensional parameters  $\kappa$  and  $m$  in the chemotactic function  $\Lambda$ . As a result, suitable estimates for these parameters would be much handy. In this regard, the behaviour of  $\Lambda$  against  $c_2$  is shown in Fig. 3a to estimate  $\kappa$  and  $m$ . Following Hillen and Painter (2009), the estimates of these parameters can be selected within the ranges of  $0 < \kappa < 1$  and  $1 < m < 3$ . The chemotactic function generally has a decreasing nature corresponding to all values within the ranges, as shown in Fig. 3a.  $\Lambda$  is plotted for three different values of  $\kappa = 0.05, 0.1, 0.2$  and  $m = 1.5, 2, 2.5$ . It is also that for higher values of  $\kappa$ , the chemotactic function decays faster; however, this decay is slow for large  $m$ . Therefore,  $\kappa = 0.1$  and  $m = 2$  could be a worthy choice.

Similarly, we go through the behaviour of the inflammatory phase net source  $\Upsilon^f$  that appears in equation (18) to estimate the value of the parameters  $s_0, s_1, s_2, s_3, s_4, s_5$  and  $s_6$  (as shown in Fig. 3b). The parameters  $s_0$  and  $s_1$  are decided inversely proportional to each other, ensuring that the first term (in the production part) of  $\Upsilon^f$ , which increases with  $c_2$ , adequately represents the growth of the inflammatory phase. Likewise,  $s_2$  and  $s_3$  are selected to be inversely proportional to each other so that the

**Table 4:** Estimated values of the non-dimensional parameters contributing in inflammatory phase source term.

Parameter	Value
$s_0$	$10^{-1}$
$s_1$	10
$s_2$	$2 \times 10^{-1}$
$s_3$	10
$s_4$	$10^{-3}$
$s_5$	$10^{-1}$
$s_6$	10

second term (in the production part) of  $\Upsilon^f$  with the growth associated with  $c_1$ , thereby justifying the observed inflammatory phase development. We consider that the death of the inflammatory phase occurs due to the toxicity of oxLDL, where  $c_1^*$  is the reference toxicity level. Consequently, the contribution of the death term (i.e. second part in  $\Upsilon^f$ ) in the inflammatory cell production increases with  $c_1$  for values higher than  $c_1^*$ . Therefore, throughout the study,  $s_4 < s_5/s_6$  can be assumed. In addition,  $s_5$  and  $s_6$  may behave inversely towards the increasing nature of the death term. Hence upon the choice of  $s_6$  within  $[1, 10]$ , it may be suitable to consider  $s_5$  in  $[0.1, 1]$  with the assumption  $s_4 < s_5/s_6$ . Also, the literature suggests that when  $s_1 = s_3 = s_6 = 0$  (first-order kinetics), the parameters  $s_0, s_2$  and  $s_5$  lies in the range  $0.1 \leq s_0, s_3 \leq 10$  (Prakash et al, 2010; Dey and Raja Sekhar, 2016). To adjust the parameter values within the specified ranges, we can consult Fig. 3b. Note that the net source term becomes negative when  $s_0, s_2 \leq s_5$ , as shown by the blue and dash-dotted lines. This incident may be physically unrealistic as the inflammatory phase forms the plaque. Hence, we can consider  $s_2 > s_5, s_0 = s_5$  with  $s_2 = 0.2, s_5 = 0.1$ , and  $s_0 = 0.1$ . In addition, in each of the following cases,  $s_3 < s_6, s_3 = s_6$  and  $s_3 > s_6$ , the corresponding scenarios are shown by the solid red, blue and black curves, respectively. Similar arguments are valid for the case  $s_3 \leq s_6$ . For simplicity, we choose  $s_3 = s_6 = 10$  following the study of Breward et al (2002) on tumor growth, and  $s_1 = 10$ , consistent with those for  $s_3$  and  $s_6$ . Finally, the value of the parameter  $s_4$  is considered as  $10^{-3}$  to satisfy the condition  $s_4 < s_5/s_6$ . The above-estimated parameter values are prescribed in Table 4.

## 6.2 Results and Discussion

This section discusses the role of the inflammatory cell phase, oxLDL, f-cytokines, and non-inflammatory phase in plaque growth. It provides a thorough analysis of the overall impact of three parameters, namely  $\nu_1, \nu_2$ , and  $\nu_3$ , on the inflammatory changes that occur in early atherosclerosis and the corresponding growth and contraction of both the inflammatory and non-inflammatory phases. It is worth noting that the inflammatory cell phase mainly contributes to plaque expansion. In Fig. 4a, we observe how the volume of inflammatory cell phase changes over time at different locations within a growing plaque. The timeline ranges from  $t_{\text{fix}} = 10$  to  $t_{\text{fix}} = 35$

and the parameters used are  $\varphi_0^f = 0.6$ ,  $\varphi^* = 0.4$ , and  $c_1^* = 0.5$ , along with other parameters selected from Tables 3 and 4. The reason for choosing the timeline range is significant and will be made clear later. The values of  $\varphi_0^f$  and  $\varphi^*$  are chosen to

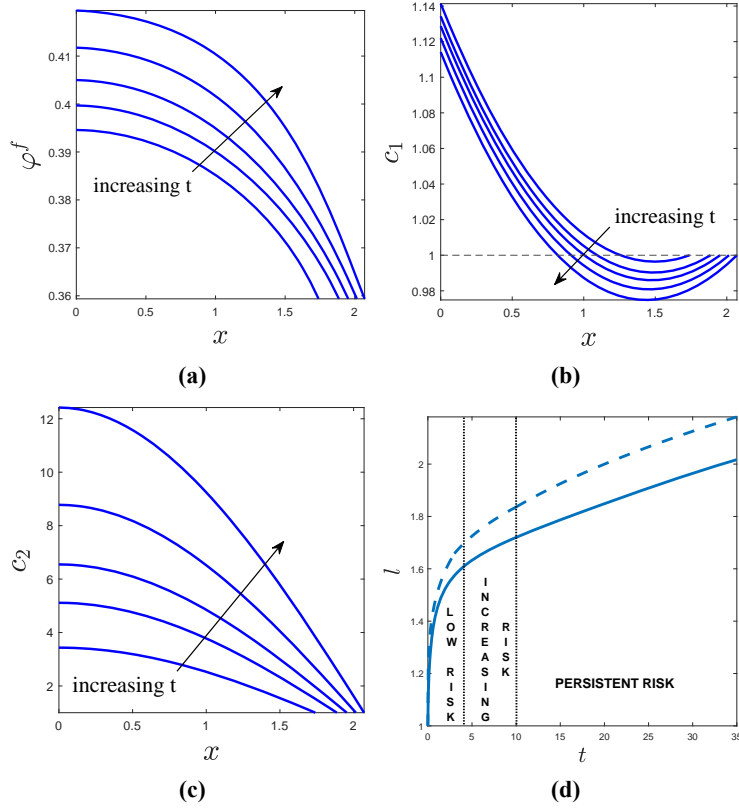


**Fig. 4:** (a) Volumetric variation of inflammatory cells, (b) OxLDL concentration, and (c) f-Cytokines (MCP-1) concentration at every locations within plaque for various  $t_{\text{fix}} = 10, 20, 25, 30$  and  $35$  at an early stage of atherosclerosis. The direction of these sequential time points is indicated by the arrows. (d) Evolution of plaque width  $l(t)$  over time  $t$ .

include cell-cell interactions initially and continue with these values, unless otherwise specified. The volume of the inflammatory cell population is found to be highest at the EII (i.e.  $x = 0$ ). Inflammatory cells accumulate mostly towards  $x = 0$ , and their volume decreases towards the moving medial boundary (or IEL boundary), i.e.,  $x = l(t)$ . Note that inflammatory cells are recruited through  $x = 0$ , resulting in a large amount of the inflammatory cell phase at that location. In due course of time, inflammatory cells gradually increase within the intima (see Fig. 4a). On the other hand, both oxLDL and f-cytokines are highly concentrated at the endothelium where

they are secreted, and their concentration decreases as one moves away from it (to affirm see the respective Fig. 4b-4c). As macrophages take in oxLDL, the number of inflammatory cells increases, causing a decrease in the concentration of oxLDL over time. However, as depicted in Fig. 4c, the concentration of f-cytokines tends to rise over time due to the secretion of these cytokines by inflammatory cells.

Evidently,  $\varphi^f$ ,  $c_1$ , and  $c_2$  are mutually dependent. Among them  $\varphi^f$  and  $c_2$  are functionally equivalent. A higher concentration of  $c_2$  within intima causes further recruitment of monocytes from the bloodstream owing to a higher outflux of f-cytokines at the EII that attract the immune cells (mainly monocytes) from the bloodstream. Therefore, their conversion into macrophages, followed by foam cells, occurs subsequently. As a result, the volumetric growth of the inflammatory cell phase is an obvious phenomenon. On the contrary, an increase in either of  $\varphi^f$  and  $c_2$  becomes responsible for the reduction in  $c_1$ . It is evident that  $\varphi^f$ ,  $c_1$ , and  $c_2$  play a collective role in the overall growth of plaque depth. Fig. 4d shows the temporal variation of plaque width, which displays a solid blue line depicting plaque width's rapid initial growth over time. Following the initial growth spurt, the growth rate decreases, although it does not exhibit an asymptotic behaviour. Hence, a question arises whether there is stability in the growth rate of plaque width. However, it is clear that the speed with which the moving edge proceeds remains almost constant after an initial period. Nevertheless, at most, three variations can be observed if we draw attention to the plaque width's behaviour with time. Such variations can be correlated with the following function proposed in this study:

$$l(t) = \begin{cases} 1 + \frac{1}{2^{\vartheta-2}} t^{\frac{1}{\vartheta+1}} & 0 < t \leq 3 \\ 1 + \varrho_1 + \frac{1}{2^{\vartheta-1}} t^{\frac{1}{\vartheta}} & 3 < t \leq 10 \\ 1 + \varrho_1 + \varrho_2 + \frac{1}{2^{\vartheta}} t^{\frac{1}{\vartheta-1}} & t > 10 \end{cases} \quad (91)$$

The values of the parameters in the above-proposed function are set as follows:  $\vartheta = 3$ ,  $\varrho_1 \in [0.29, 0.3]$  and  $\varrho_2 \in [0.14, 0.15]$ , to ensure that the correlation becomes a reliable approximation of the plaque growth curve. Note that the number of variation zones in the growth curve is the same as the value of  $\vartheta$ . The dotted line in Fig. 4d represents the growth curve corresponding to the above-proposed correlation (91). The similarity in behavior between the two lines in Fig. 4d indicates that Eq. (91) is a reliable approximation of the solid line, which represents the plaque growth curve in this study. We are able to identify three distinct natures within the plaque growth curve, which correspond to the three stages of early atherosclerosis: low risk, increasing risk and persistent risk. We show the corresponding zone classification with two vertical dotted straight lines. It is worth noting that the parabolic nature of the plaque growth curve beyond  $t = 10$  implies the risk of developing complications related to atherosclerosis in a patient. As soon as the plaque depth attends such a parabolic nature with time, atherosclerosis is expected to continue for a patient unless it is being treated. Hence, we should give importance on the simulated results beyond  $t > 10$  days only. Accordingly, we choose [10, 35] days as the range of time for our study. The parabolic nature indicates the inhibition of plaque growth due to the experience of normal stress from its surroundings within the intima. The impact of oxLDL-induced toxicity on plaque growth is significant. Further details regarding this matter are discussed

in the subsequent sections. According to this model, early atherosclerotic plaque expands towards the internal elastic lamina (IEL) and in reality, this is also the case. The growing plaque experiences a more considerable rigidity from IEL compared to the damaged endothelium. As a result, in later stages, the ever-increasing plaque has no way except to enter the lumen after causing further damage to the endothelium. This is why atherosclerosis narrows the lumen to prevent blood flow.

Within the intima, macrophages (differentiated from monocytes) consume oxLDL to become lipid-laden foam cells, and both macrophages and foam cells co-exist as the inflammatory cell phase. Consequently, the volume fraction of the inflammatory cell phase depends on oxLDL concentration. Although the reason for macrophage and foam cell death within the intima has not been studied immoderately, a few studies suggest that the toxicity due to the overconsumption of oxLDL is responsible for the death (Hegyí et al, 1996; Marchant et al, 1996; Liu et al, 2008). Therefore, we take into consideration the occurrence of inflammatory cell death caused by oxLDL-induced toxicity beyond the value  $c_1 = c_1^*$  as explained in equation (18). Fig. 5a depicts the variation of inflammatory cell volume with oxLDL concentration when  $c_1^* = 1.05$  (oxLDL induced reference toxicity level) at various time  $t$ . Accordingly, we fix  $t = t_{\text{fix}}$  where  $t_{\text{fix}} = 10, 15, 20, 25$  etc. Corresponding to each  $t_{\text{fix}}$ , one can identify  $\varphi^f$  and  $c_1$  as the function of  $x(t = t_{\text{fix}})$  such that for each  $t = t_{\text{fix}}$  we get both the values of  $\varphi^f$  and  $c_1$  at each point of the plaque. Evidently, the data-set  $(c_1, \varphi^f) = (1, 0.36)$  corresponds to the plaque boundary. Initially, the inflammatory cell population increases with  $c_1$  as the consumption of oxLDL produces them. Subsequently, the death of inflammatory cells starts due to  $c_1$  exceeding  $c_1^*$ . Consequently, the increasing nature of  $\varphi^f$  ceases, and it saturates to a nearly constant value (Fig. 5a). Moreover, this figure enables us to detect two different values of  $\varphi^f$  corresponding to  $c_1 = 1$  for each  $t = t_{\text{fix}}$ . The occurrence of two different values of  $\varphi^f$  corresponding to the same  $c_1$  (in particular, the magnitude of  $c_1$  at the plaque moving boundary) takes place due to the triggering of oxLDL induced toxicity. To be precise, an increase in the accumulation of oxLDL at any location within the intima leads to a significant increase in foam cell proliferation. This incident, in turn, results in toxicity towards the foam cell population, reducing the foam cell volume. On the other hand, the dead foam cells release an excess amount of oxLDL into the intima to increase its concentration as a repercussion.

At various instants of time, the variation of  $\varphi^f$  shows diverse behavior at different location within the intima depending upon the value of the parameters chosen for our discussion. Similar incident is expected for  $c_1$  and  $c_2$ . Therefore for the sake of convenience, it decided to integrate  $\varphi^f$ ,  $c_1$ , and  $c_2$  within the range  $[0, l(t)]$  to obtain the following volume averaged variables respectively:

$$\text{Averaged Volume of Inflammatory Cells} : \langle \varphi^f \rangle = \frac{1}{l(t)} \int_{x=0}^{l(t)} \varphi^f(x, t) dx, \quad (92a)$$

$$\text{Averaged oxLDL Concentration} : \langle c_1 \rangle = \frac{1}{l(t)} \int_{x=0}^{l(t)} c_1(x, t) dx, \quad (92b)$$

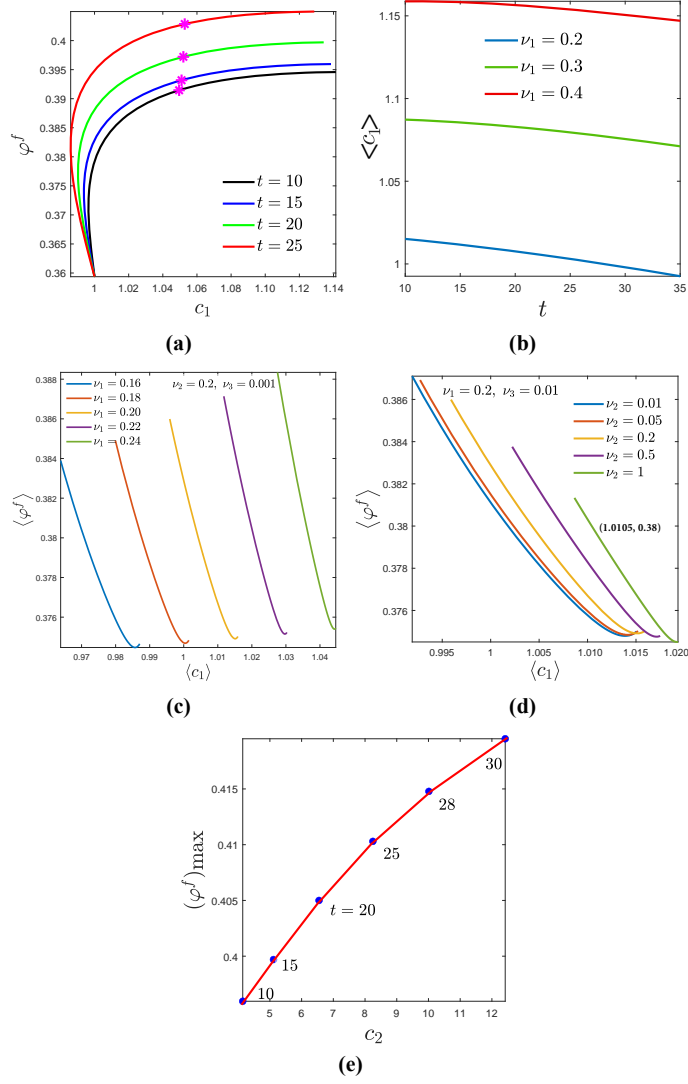


**Fig. 5:** (a) Inflammatory cell volume variation with oxLDL concentration, (b) Average oxLDL concentration for various  $\nu_1$  when  $\nu_2 = 0.01$  and  $\nu_3 = 0.01$ , (c) Average volume fraction of inflammatory cells varies with average oxLDL concentration for different  $\nu_1$ , (d) Average volume fraction of inflammatory cells with variation in average oxLDL concentration for various  $\nu_2$ , (e) Maximum volume fraction of inflammatory cells at different times with respect to f-cytokines concentration. The star markers in (a) indicate the volume fraction of inflammatory cells corresponding to  $c_1^* = 1.05$ , and the blue dots in (d) represent the maximum volume of inflammatory cells corresponding to  $t = 10, 15, 20, 25, 28, 30$ .

and

$$\text{Averaged f-cytokines Concentration : } \langle c_2 \rangle = \frac{1}{l(t)} \int_{x=0}^{l(t)} c_2(x, t) dx. \quad (92c)$$

Henceforth, most of the discussion has been done regarding the above-averaged quantities. The integrals at the right-hand side of the above equations are evaluated using standard Newton's cotes formulae. The numerical solutions of  $\varphi^f$ ,  $c_1$ , and  $c_2$  are subjected to Simpson's 1/3 rule within the interval  $[0, l(t)]$  for each  $t \in [0, T]$ . The values of  $\langle \varphi^f \rangle$ ,  $\langle c_1 \rangle$ , and  $\langle c_2 \rangle$  are functions of time  $t$ . These quantities may exhibit unstable behaviour at the onset of the inflammatory process. Sometimes, even a small deviation in the parameter value can result in a significant variation in magnitude. Consequently, it is imperative to show the graphical simulations some time steps later. Eventually, we choose a time interval of  $[10, 35]$  days to generate graphical results. Fig. 5b displays the temporal variation of average oxLDL concentration within time domain  $[10, 35]$  days corresponding to different influx rates  $\nu_1 = 0.2, 0.3, 0.4$ . The parameter  $\nu_1$  represents constant oxLDL influx into the intima through damaged endothelium. According to [Chalmers et al \(2015\)](#),  $\nu_1$  can be considered proportional to the blood LDL level. LDL molecules enter the intima through damaged endothelium, where free oxygen radicals oxidize them to become oxLDL. This oxidation process is speedy. The timescale for oxidation is infinitesimally small compared to plaque growth. Thus, it is more accurate to assume that oxLDL enters the intima from the lumen through the EII ( $x = 0$ ) rather than free lipids (LDL) influx. The concentration of oxLDL enhances throughout the intima due to the flux parameter  $\nu_1$  that takes only a positive value. However, over time, the average oxLDL concentration  $\langle c_1 \rangle$  reduces. With reducing  $\nu_1$ , a higher rate of decay of  $\langle c_1 \rangle$  is realized. The reduced influx rate of oxLDL corresponds to the situation when the endothelium layer suffers minor damage. Similarly, a larger influx rate of oxLDL can be correlated with a major damaged endothelium.

In Fig. 5c, we can see a relationship between the average volume of inflammatory cells, denoted by  $\langle \varphi^f \rangle$ , and the average concentration of oxLDL, represented by  $\langle c_1 \rangle$ , for the values of  $\nu_1 = 0.16, 0.18, 0.20, 0.22, \text{ and } 0.24$ . The results show that for a particular  $\nu_1$ ,  $\langle \varphi^f \rangle$  decreases with enhanced  $\langle c_1 \rangle$  over time. However, increased magnitude of both the maximum and minimum value of  $\langle \varphi^f \rangle$  with higher influx rate suggests a larger accumulation of inflammatory cells within the intima. Thus,  $\nu_1$  plays a positive role in the recruitment process of inflammatory cells from the lumen. If we associate an elevated influx of oxLDL with increased damage in the endothelium, the intima is found to gather a larger volume of inflammatory cells. The only known cause for the inverse relationship between  $\langle \varphi^f \rangle$  and  $\langle c_1 \rangle$  when the oxLDL influx rate is fixed is oxLDL-induced toxicity. On the other hand, as shown in Fig. 5d,  $\nu_2$  is responsible for decreasing the maximum value of  $\langle \varphi^f \rangle$ . To assess the impact of  $\nu_2$  on  $\langle c_1 \rangle$  and  $\langle \varphi^f \rangle$ , a fixed point  $(1.0105, 0.38)$  on the curve corresponding to  $\nu_2 = 1$  (green line in Fig. 5d) is chosen. When  $\langle \varphi^f \rangle$  is held constant at 0.38, an increase in  $\nu_2$  leads to an improvement in  $\langle c_1 \rangle$ . Consequently, an enhancement in  $\langle \varphi^f \rangle$  is expected owing to a hike in  $\nu_2$  (for a quick review, one can fix  $\langle c_1 \rangle = 1.0105$  on the green line i.e., corresponding to  $\nu_2 = 1$ ). The (in)flux of f-cytokines is controlled by  $\nu_2$ , which depends on the concentration

of oxLDL at the EII. The recruitment of inflammatory cells is directly affected by the flux of f-cytokines. Therefore, an increase in the average concentration of oxLDL (i.e.,  $\langle c_1 \rangle$ ) within the intima would intensify the recruitment of inflammatory cells. In other words, an increase in the average volume of inflammatory cells within the intima indicates a rise in the average concentration of oxLDL within the intima when the toxicity impact is not taken into consideration. A detailed discussion of this matter

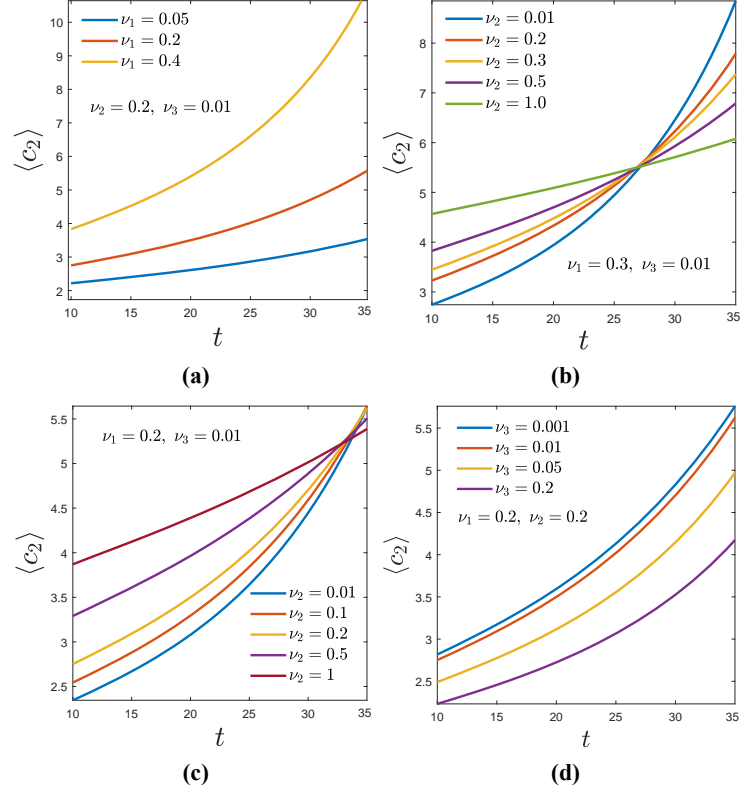


**Fig. 6:** Average f-cytokines concentration ( $\langle c_2 \rangle$ ) versus  $t$  (in days) for various (a)  $\nu_1$  (when  $\nu_2 = 0.2$  and  $\nu_3 = 0.01$ ), (b)  $\nu_2$  (when  $\nu_1 = 0.3$  and  $\nu_3 = 0.01$ ), (c)  $\nu_2$  (when  $\nu_1 = 0.2$  and  $\nu_3 = 0.01$ ), and (d)  $\nu_3$  (when  $\nu_1 = 0.2$  and  $\nu_2 = 0.2$ ).

is overdue and has been reported in this section of the manuscript. However, it is essential to note the impact of f-cytokines on the inflammatory cell volume within the intima. We would like to see the maximum possible recruitment of inflammatory cells within the intima being regulated by the f-cytokines concentration at various locations within the atherosclerotic plaque. The maximum growth of inflammatory cells, denoted by  $(\varphi^f)_{\max}$ , occurs at an individual time  $t = t_{\text{fix}}$ . Note that  $c_1$  affects the concentration of f-cytokines ( $c_2$ ), which is responsible for the transmigration of monocytes or macrophages into the intima, resulting in the formation of foam cells.

The concentration of f-cytokines, in turn, influences the production of inflammatory cells. In this modelling, we consider this fact in terms of the boundary condition (60). Fig. 5e shows the locus of  $(\varphi^f)_{\max}$  concerning f-cytokines concentration for each  $t_{\text{fix}} = 10, 15, 20, 25$  (each blue dot represents the value for the corresponding time that is indicated). The maximum growth of the inflammatory cell population is expected to reach a stable state. In the next section, we will discuss the impact of f-cytokines influx parameters on plaque development.

### 6.2.1 The Role of f-Cytokines Influxes $\nu_2$ and $\nu_3$ on the Plaque Growth Behaviour

When the concentration of oxLDL increases within the intima, f-cytokines control the migration of macrophages into the intima. The amount of f-cytokines flux at the EII is directly proportional to the concentrations of oxLDL and f-cytokines according to boundary condition (60). Note that f-cytokines are primarily produced by endothelial cells, and its flux is regulated by the parameters  $\nu_2$  and  $\nu_3$ .  $\nu_2$  is responsible for connecting the influx of f-cytokines with oxLDL concentration at the EII, while  $\nu_3$  regulates the outflux of f-cytokines by controlling their concentrations at the interface. The influx of oxLDL, governed by the parameter  $\nu_1$ , plays a crucial role in hiking the concentration of f-cytokines within the intima, as shown in Fig. 6a. In addition,  $\nu_1$  also determines the release of f-cytokines from endothelial cells and foam cells, thereby supporting the recruitment of monocytes (macrophages derived from monocytes) from the bloodstream to the intima. Therefore, the parameter  $\nu_1$ , which controls the influx of oxLDL and the average oxLDL concentration within the intima, also affects the influx rate of f-cytokines as per the interface condition (60). This condition is also insinuating the influences of  $\nu_2$  and  $\nu_3$  to evolve oxLDL and f-cytokines respectively at the EII. Fig. 6b illustrates five variations of the average f-cytokines concentration against time within the range  $t \in [10, 35]$  corresponding to  $\nu_2 = 0.01, 0.2, 0.3, 0.5, 1$  when  $\nu_1 = 0.3$  and  $\nu_3 = 0.01$ . Larger  $\nu_2$  regulates the flux of f-cytokines at EII to increase average concentration within intima until a specific time  $t = t^*$  (here  $t^* \approx 27$  days), after which the situation reverses. When  $t < t^*$  days, a higher magnitude of  $\nu_2$  assists the first term at the right-hand side of (60) to dominate over the second one. As a result, a higher influx of f-cytokines developed at the EII, consequently enhancing average f-cytokines concentration inside the intima. However, beyond  $t = t^*$  days, the second term of (60) dominates over the first term. In this situation, over time the influx of f-cytokines changes to an outflux, causing a depletion in the average concentration of f-cytokines within the intima. Such an outflux further assists in recruiting monocytes/macrophages from the bloodstream. The occurrence of  $t^*$  gets delayed at to a lower magnitude of  $\nu_1$ . In other words, corresponding to a lower-level of damage in endothelium, the generation of f-cytokines outflux becomes delayed. As a result, the inflammatory response in the form of monocytes recruitment gets delayed. Obviously, a higher-level damage in endothelium causes a quicker inflammatory response by the immune cells in bloodstream. This fact can be illustrated through the Fig. 6c which shows  $t^* \approx 32$  days when  $\nu_1 = 0.2$  and  $0.5 \leq \nu_2 \leq 1$ . A further delay in the occurrence of  $t^*$  can be noticed when  $0.01 \leq \nu_2 \leq 0.2$ . Definitely, a higher flux of f-cytokines prevails at the EII when

$0.5 \leq \nu_2 \leq 1$  as compared to the situation when  $0.01 \leq \nu_2 \leq 0.2$ . The parameter  $\nu_3$  which basically controls the outflux of f-cytokines, produces higher outflux at larger magnitude of  $\nu_3$ . Fig. 6d depicts four variations of  $\langle c_2 \rangle$  against time within the range  $t \in [10, 35]$  when  $\nu_3 = 0.001, 0.01, 0.05, 0.1$  and  $\nu_1 = \nu_2 = 0.2$ . Consequently, this graphical result confirms that the average concentration of f-cytokines becomes high within the intima when  $\nu_3$  produces a minimal outflux.

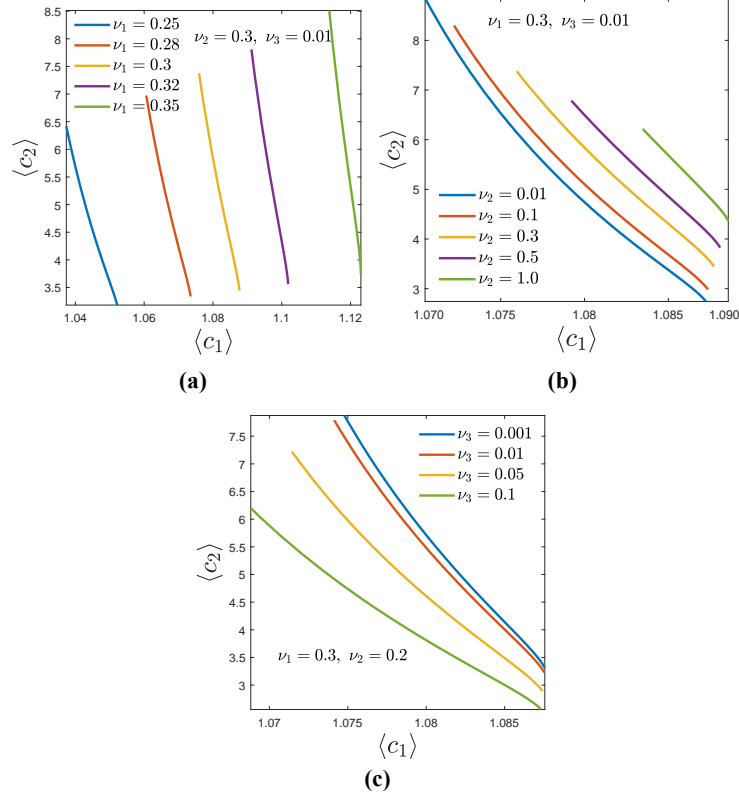


**Fig. 7:** Variation of average f-cytokines concentration with average oxLDL concentration corresponding to various (a)  $\nu_1$  (when  $\nu_2 = 0.3$  and  $\nu_3 = 0.01$ ), (b)  $\nu_2$  (when  $\nu_1 = 0.3$  and  $\nu_3 = 0.01$ ) and (c)  $\nu_3$  (when  $\nu_1 = 0.3$  and  $\nu_2 = 0.2$ ).

Based on our previous discussion, it is clear that f-cytokines and oxLDL have a mutual impact that can be discussed in terms of the influx/outflux parameters  $\nu_1, \nu_2$  and  $\nu_3$ . Fig. 7a-7c display the variation of average f-cytokines ( $\langle c_2 \rangle$ ) concentration in reference to the average oxLDL concentration ( $\langle c_1 \rangle$ ) corresponding to influx/outflux parameters  $\nu_1, \nu_2$  and  $\nu_3$  respectively. Both the  $\langle c_1 \rangle$  and  $\langle c_2 \rangle$  are functions of time. These figures demonstrate that when  $\nu_1, \nu_2$ , and  $\nu_3$  are held fixed, a reciprocal

relationship between  $\langle c_1 \rangle$  and  $\langle c_2 \rangle$  over time is evidenced. Over time, as the concentration of average oxLDL increases within the intima, foam cells and endothelium release f-cytokines to recruit immune cells, mainly monocytes, from the bloodstream. As a result, one can expect an outflux of f-cytokines from the intima to the lumen, which is responsible for the decrease in f-cytokines concentration, in addition to the growth of oxLDL within the intima over time. If  $\nu_1 = 0$  corresponds to an undamaged endothelium, we may designate the constant  $\nu_1$  as the static damage (no further damage is expected) in the endothelium. In that undamaged situation, the inflammatory response becomes limited. oxLDL enriches the production of f-cytokines at the endothelium that is characterised by  $\nu_2$ . An increasing  $\nu_2$  suggests more f-cytokines within intima, which is consistent with the earlier result (Fig. 6b-6c). Beside the endothelium, inflammatory cells population is also a source of f-cytokines within the intima. Increased oxLDL concentration induces toxicity towards the inflammatory cells and it remains the primary cause of the death of inflammatory cells. Due to the increased population of dead foam cells, the number of available inflammatory cells to produce f-cytokines becomes less. Consequently, the oxLDL induced toxicity affects average concentration of f-cytokines ( $\langle c_2 \rangle$ ) which is an inflammatory marker. On the contrary, a hike in  $\nu_1$  corresponds to more serious damage in the endothelium, which is attributed to an upsurge in oxLDL influx at EII. Definitely, both  $\langle c_1 \rangle$  and  $\langle c_2 \rangle$  rise with increasing damage of endothelium. Precisely, both the maximum and minimum of  $\langle c_2 \rangle$  are enhanced with  $\nu_1$  (see Fig 7a). However, the maximum of  $\langle c_2 \rangle$  reduces with  $\nu_2$  but the minimum of  $\langle c_2 \rangle$  shows an opposite nature (see Fig. 7b). At a higher magnitude of  $\nu_2$ , the impact of the first term of (60) can easily dominate the second one. Consequently, due to the increased influx of f-cytokines at EII,  $\langle c_2 \rangle$  goes higher. However, as discussed earlier, at this elevated level,  $\langle c_1 \rangle$  continues to reciprocate with  $\langle c_2 \rangle$  due to the impact of oxLDL-induced toxicity. A reduction in the maximum of  $\langle c_2 \rangle$  and enhancement of minimum of  $\langle c_2 \rangle$  within the intima corresponding to the higher magnitude of  $\nu_2$  leads to the situation when there is a decreased outflux of f-cytokines. Hence, the recruitment of inflammatory cells gets delayed, leading to an increase in  $\langle c_1 \rangle$  within the intima. In addition to the oxLDL-induced toxicity, the increasing f-cytokines outflux parameter  $\nu_3$  (where  $\nu_3 = 0.001, 0.01, 0.05, 0.1$ ) is behind the reduction of  $\langle c_2 \rangle$  as demonstrated in Fig. 7c. On the contrary, excessive outflux of f-cytokines results in a more inflammatory response and, consequently, the higher recruitment of monocytes-derived macrophage into the intima has resulted. This excess amount of macrophages now consumes the available oxLDLs, reducing its average concentration within the intima.

It is worth noting that inflammatory cells primarily contribute to early plaque development. Therefore, we must emphasize the roles of influx/outflux parameters  $\nu_1$ ,  $\nu_2$ , and  $\nu_3$  on the average volume of inflammatory cells  $\langle \varphi^f \rangle$ . In this regard, Fig. 8a-8c depict the individual impacts of  $\nu_1$ ,  $\nu_2$ , and  $\nu_3$  on  $\langle \varphi^f \rangle$  respectively. In all these three cases, the average volume of foam cells grows with  $t$  within a given interval [10, 35].  $\nu_1$ , which corresponds to the influx of oxLDL, becomes responsible for foam cell production. Higher oxLDL concentrations trigger an inflammatory response, drawing new inflammatory cells to the intima from the bloodstream. As a result, one can

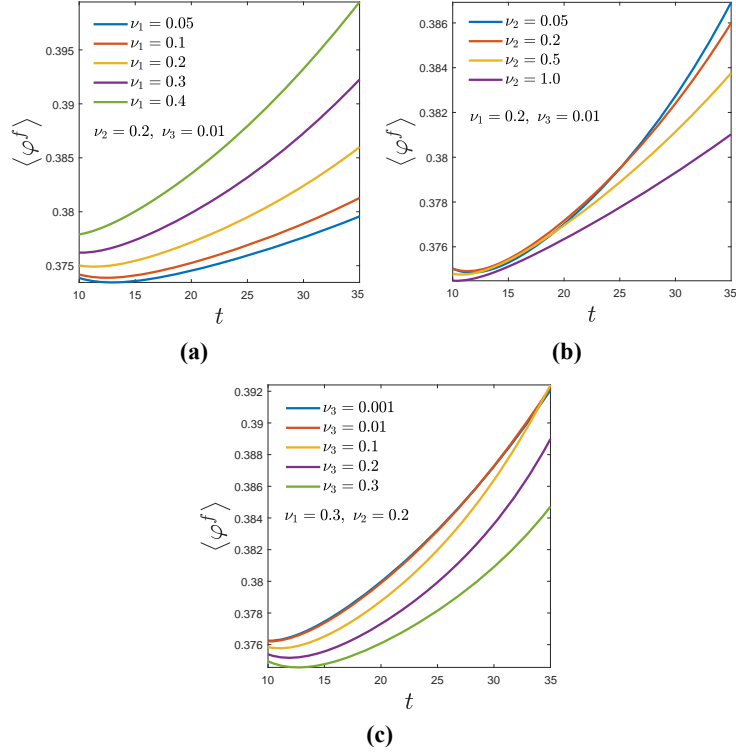


**Fig. 8:** Variation of inflammatory cell average volume fraction for different (a)  $\nu_1$ , (b)  $\nu_2$ , and (c)  $\nu_3$ .

expect higher foam cell production. Fig. 8a supports this phenomenon. However, another influx parameter  $\nu_2$  is found to show an alternating behavior towards  $\langle \varphi^f \rangle$ . Corresponding to  $\nu_2 = 0.05, 0.2, 0.5, 1$ , a reduction in  $\langle \varphi^f \rangle$  is evidenced in Fig. 8b. One may ask whether  $\nu_2$  has a preventive role in overall plaque development. Therefore, we need to look for an appropriate answer. It is already been investigated that  $\nu_2$  has a positive role in the increase in average f-cytokines concentration within intima up to a certain time. Moreover, the outflux of f-cytokines becomes limited at higher  $\nu_2$ . As a result, a restricted recruitment of additional inflammatory cells is expected. Subsequently, fewer inflammatory cells are available to consume oxLDL. Besides,  $\nu_3$  shows an impact on  $\langle \varphi^f \rangle$  which appears to be a preventive towards the growth of  $\langle \varphi^f \rangle$ . Fig. 8c illustrates a loss in the average volume of inflammatory cells for an increased  $\nu_3$ . As discussed earlier, a higher magnitude of  $\nu_3$  causes a better outflux of f-cytokines. Consequently, one would expect a boost in the recruitment of inflammatory cells. Nevertheless, a diminishing behavior in  $\langle \varphi^f \rangle$  is noticed with elevated  $\nu_3$ . The possible reason behind this phenomenon is oxLDL-induced toxicity. Based on the prior studies,  $\nu_1/\nu_3 \sim \mathcal{O}(10^0)$  is reported in the Table 3 of this present article. Consequently, the influence of  $\nu_1$  is expected to be more significant

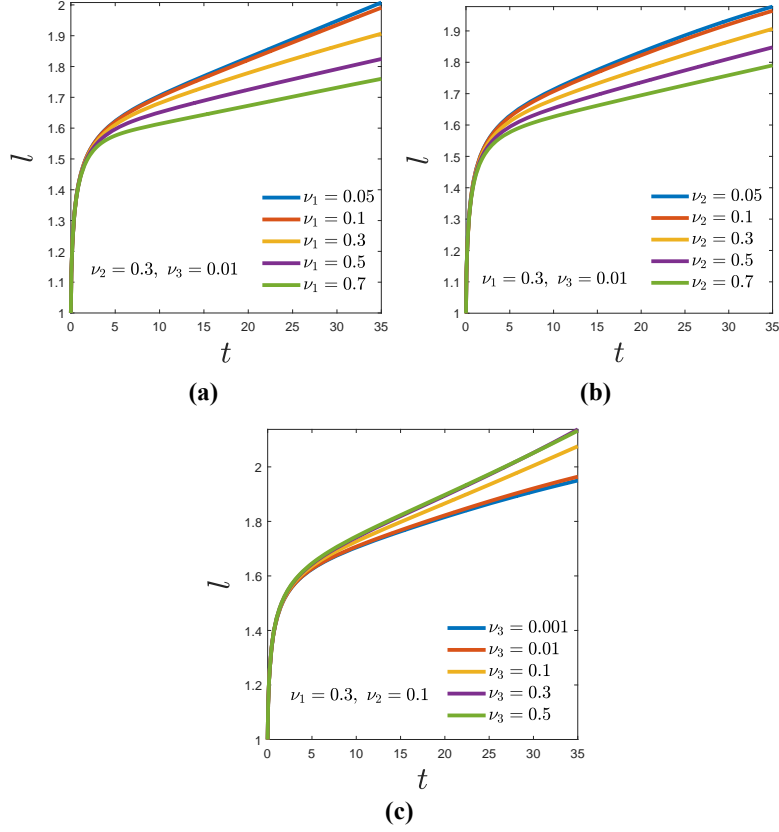


**Fig. 9:** Plaque width for various (a)  $\nu_1$ , (b)  $\nu_2$ , and (c)  $\nu_3$ .

than  $\nu_3$ . As a result, the impact of oxLDL-induced toxicity suppresses the enhanced migration of inflammatory cells. In other words, the population of new inflammatory cells corresponding to higher  $\nu_3$  are inadequate to consume the available oxLDL due to the influx parameter  $\nu_1$ . Correspondingly, the excess oxLDL becomes toxic to the inflammatory cells. Later, we would like to study the growth of  $l(t)$  for various influx/outflux parameters for a comprehensive explanation.

As noted earlier, early plaque development primarily depends on the inflammatory cell phase in the presence of oxLDL molecules within the intima and active f-cytokines gradient. Consequently, the plaque width is controlled by  $\nu_1$ ,  $\nu_2$  and  $\nu_3$  depicted through Fig. 9a-9c respectively. We identify three separate regimes of early atherosclerosis: low risk, increasing risk and persistent risk. These three parameters mainly affect the third regime. Hence, one can comprehend the long-term impact of these parameters. Elevating  $\nu_1$  leads to a significant increase in oxLDL within the intima layer. However, the curve  $l(t)$  moves closer to the  $t$ -axis at a higher time level. The persistent risk regime narrows down at a higher  $\nu_1$  magnitude. It doesn't mean

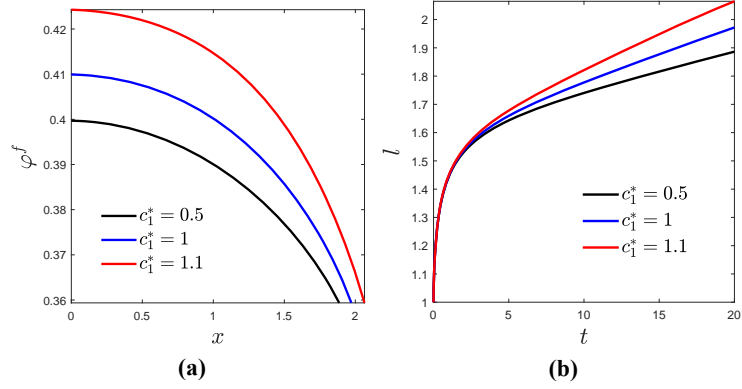


**Fig. 10:** (a) Distributions of inflammatory cell volume fraction, and (b) plaque width variation with  $t$  within the intima corresponding to various  $c_1^*$ .

that at a higher  $\nu_1$ , the overall process of atherosclerosis becomes retarded. A higher influx parameter  $\nu_1 > 0.1$  inevitably results in a significant buildup of foam cells in the intima. Further, oxLDL-induced toxicity prevents such accumulation because of foam cell death. The free oxLDLs released from the dead foam cells cause further recruitment of new inflammatory cells. Consequently, the overall inflammatory process persists, leading to a stable plaque growth process. On the other hand, with a low influx rate of oxLDL, the impact of induced toxicity becomes marginal over the foam cell population. When the oxLDL influx rate  $\nu_1 \leq 0.1$ , a marginal change in the plaque depth happens for a further lower magnitude of  $\nu_1$ . In this situation, the foam cells deposited within the intima (though not a big number) do not encounter the toxicity effect much. Moreover, the number of recruited inflammatory cells goes down with further smaller  $\nu_1$  less than 0.1. Over time, the plaque depth increases sharply. Now the regime of persistent risk becomes wider. It is important to note that the growth rate of plaque tends to slow down unless sufficient dead materials are produced from the inflammatory cells. However, this aspect is outside the scope of the current study. As a result, the advancement of plaque growth gets delayed in advanced stages. The present study shows that oxLDL-induced toxicity is a critical factor in the stability of plaque growth.

The role of cytokines influx and outflux parameters  $\nu_2$  and  $\nu_3$  respectively are found to reciprocally behave over the plaque growth. The impact of  $\nu_2$  on the plaque growth profile is found to be similar with  $\nu_1$  (see Fig. 9b). In addition, it is observed that the plaque growth rate ceases for further smaller value of  $\nu_2$  less than 0.1. When  $\nu_3 = 0.01$  and  $\nu_2 \geq 0.1$ , the f-cytokines influx dominates the outflux. This dominance in f-cytokines influx could reduce the necessity for recruiting new inflammatory cells. Consequently, the plaque growth rate tends to stabilize, analogous to the scenario evident in the toxic impact of oxLDL, potentially leading to a stable state. However, the said f-cytokines outflux dominates the influx when  $\nu_2 = 0.1$  and  $0.01 \leq \nu_3 \leq 0.3$ . In this situation, inflammatory cells are inadequate inside the intima; however, the

oxLDL concentration is up to the mark. Hence, further recruitment of inflammatory cells is necessitated, leading to an elevated growth rate in plaque depth (see Fig. 9c). It is also noticed that the domination of the outflux over the influx of f-cytokines becomes ineffective when  $\nu_3 > 0.3$  and  $\nu_2 = 0.1$ . On the other hand, the domination of the influx over the outflux of f-cytokines terminates when  $\nu_3 < 0.01$  and  $\nu_2 = 0.1$ . Consequently, the effective range for  $\nu_3$  is  $0.01 \leq \nu_3 \leq 0.3$  when  $\nu_2 = 0.1$  and  $\nu_1 = 0.3$ . This range may vary depending on the magnitudes of  $\nu_1$  and  $\nu_2$ . The comprehensive analysis affirms that the influx parameters  $\nu_1$  and  $\nu_2$  corresponding to oxLDL and f-cytokines, respectively, positively influence the stable plaque growth process, primarily attributed to oxLDL-induced toxicity. On the other hand, the outflux parameter  $\nu_3$  associated with f-cytokines disrupts the stability.

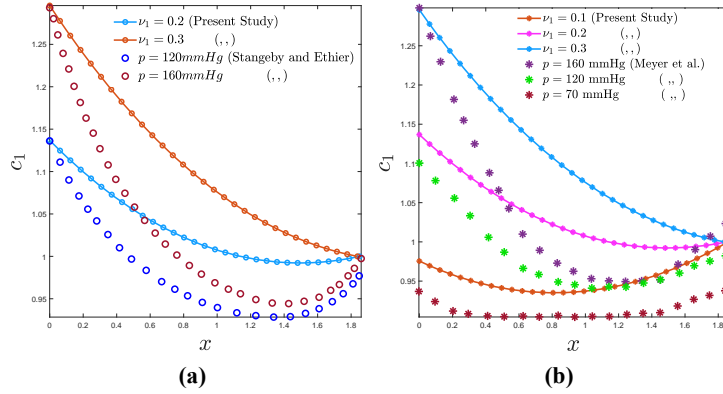


**Fig. 11:** Comparison between the present study and the clinical studies done by (a) [Stangeby and Ethier \(2002\)](#) and (b) [Meyer et al \(1996\)](#) along the variation of oxLDL concentration with distance from the intima-endothelium interface corresponding to various  $\nu_1$  for different pressures.

### 6.2.2 Effect of Toxicity Level Induced by oxLDL ( $c_1^*$ )

As discussed earlier, the toxicity caused by oxLDL leads to inflammatory cell death, which in turn contributes significantly to the plaque formation. The impact of different toxicity levels, denoted by  $c_1^*$ , on the growth of inflammatory cell volume and plaque width, is shown in Fig. 10a-10b respectively. Inflammatory cells are destroyed when oxLDL reaches its toxicity level. Higher toxicity levels result in more inflammatory cell growth due to their rapid proliferation and absence of death up to that level. This incident leads to an increase in the volume fraction of inflammatory cells as  $c_1^*$  rises (Fig. 10a). Additionally, an increase in  $c_1^*$  leads to an increase in plaque width, as shown in Fig. 10b. As the population of inflammatory cells grows with a higher  $c_1^*$ , the plaque, formed by the deposition of inflammatory cells, develops more quickly.

### 6.3 Qualitative Agreement with the Clinical Studies

We have attempted to compare specific results from this study with the existing clinical studies done by Meyer et al (1996) and Stangeby and Ethier (2002). Accordingly, the LDL concentrations within the arterial intima are picked up from these studies corresponding to transmural pressures of  $p = 70, 120, 160$  mmHg. The LDL concentration data are extracted using the ‘Grabit’ toolbox of MATLAB R2021a. They are normalized first before comparing with the oxLDL concentrations obtained from the present study at each point within the intima. The normalization process is done so that the domain of clinical data maps onto that of the present study through a suitable transformation. Such transformation enables us to focus more on the qualitative agreement rather than the quantitative. Note that the present study is focused on oxLDL rather than LDL as the oxidization takes place in a short time while growth is a long time scale process. Figs. 11a and 11b delineate the above-mentioned comparative study. In the first plot, the concentrations of oxLDL (this study) and LDL (Stangeby and Ethier (2002)) are shown for  $\nu_1 = 0.2, 0.3$  and  $p = 120, 160$ , respectively. The following figure compares the present study and Meyer et al (1996), corresponding to  $\nu_1 = 0.1, 0.2, 0.3$  and  $p = 70, 120, 160$  respectively. A good qualitative agreement between the clinical and present studies has been observed, and the comparisons show that the normalized LDL (obtained from Meyer et al (1996) and Stangeby and Ethier (2002)) and oxLDL (obtained from the current study) concentrations behave similarly. Both are highly concentrated near the lumen or EII and decrease toward the media or arterial wall.

## 7 Summary and Conclusions

Multiphase mixture theory models are adopted to investigate the role of macrophages and foam cells in the early stages of atherosclerosis. This study found that oxLDL-induced toxicity plays a significant role in the early growth of plaque. Macrophages consume oxLDL to become foam cells, but overconsumption causes toxicity, which can lead to the death of foam cells. The study systematically analyzed the activity of oxLDL, the role of f-cytokines, and the behavior of inflammatory cells, such as foam cells and macrophages. Plaque growth is limited to the intima and is subjected to constant inward normal stress from the surrounding intima materials and internal elastic lamina. The study identified three regions corresponding to early plaque growth: low risk, increasing risk, and persistent risk. The growth is initially steep but gradually stabilizes into a parabolic profile due to the oxLDL-induced toxicity effect. Furthermore, the toxic effect of oxLDL impacts the functioning of inflammatory cells and f-cytokines. Correspondingly, a correlation (91) is proposed that dictate the plaque growth process when oxLDL induced toxicity issue is taken into the consideration.

This study introduces three parameters that determine the in and out fluxes of substances in the plaque. These parameters are called  $\nu_1, \nu_2$ , and  $\nu_3$ . The first parameter,  $\nu_1$ , is associated with the influx of oxLDL, while the second and third parameters,  $\nu_2$  and  $\nu_3$ , correspond to the influx and outflux of f-cytokines, respectively. When there is a high influx of oxLDL, it leads to greater stability in the plaque width profile. However, a high influx of oxLDL also increases the risk of oxLDL-induced toxicity,

which can stabilize the growth rate of the plaque. The f-cytokines influx parameter,  $\nu_2$ , behaves similarly to the oxLDL influx parameter over plaque development. Both these parameters are responsible for the growth of foam cells. However, the influx and outflux parameters corresponding to f-cytokines have a reciprocal effect on plaque growth. The analysis indicates that the influx parameters have a positive influence on the stability of the plaque growth process, whereas the outflux parameter associated with f-cytokines destabilizes the growth. Furthermore, the outflux parameter  $\nu_3$  for f-cytokines can diminish the overall inflammatory process by decreasing the recruitment of inflammatory cells from the bloodstream to the intima layer through the damaged endothelium. Moreover, we observed a significant change in the plaque growth profile due to the variation in the toxicity level,  $c_1^*$ . A higher toxicity level indicates mainly the death of foam cells and the proliferation of more inflammatory cells, accelerating plaque growth.

The present study simplifies several complex mechanisms involved in early atherosclerosis to understand plaque formation. It is illustrated that plaque formation relies on oxLDL ingestion and macrophage chemotaxis. The role of oxLDL toxicity in plaque growth is established. This study would help in developing new therapeutic strategies to prevent the progression of atherosclerosis in its early stages. Additionally, the impact of High-density lipoprotein (HDL) on plaque development may be even more significant in the presence of oxLDL-induced toxicity.

## Acknowledgements

First author A. S. Pramanik acknowledges University Grants Commission (UGC), Govt. of India for providing Senior Research Fellowship (NET-JRF, Award Letter Number: 1149/(CSIR-UGC NET DEC-2018)). Second author B. Dey acknowledges University Research Assistance (Ref. 1516/R-2020 dated 01.06.2020) of University of North Bengal for supporting this work.

## Appendix A: Leading order coefficients

$$(\varphi^n)^{(0)} = 1 - (\varphi^f)^{(0)},$$

$$\Upsilon^f{}^{(0)} = (\varphi^f)^{(0)}(\varphi^n)^{(0)} \frac{s_0 c_2^{(0)}}{1 + s_1 c_2^{(0)}} + (\varphi^f)^{(0)}(\varphi^n)^{(0)} \frac{s_2 c_1^{(0)}}{1 + s_3 c_1^{(0)}} - (\varphi^f)^{(0)} \frac{s_4 + s_5 c_1^{(0)}}{1 + s_6 c_1^{(0)}} \mathcal{H}(c_1^{(0)} - c_1^*),$$

$$Q_1^{(0)} = (\varphi^f)^{(0)}(\varphi^n)^{(0)} q_0 c_1^{(0)} - (\varphi^f)^{(0)}(\varphi^n)^{(0)} q_2 c_1^{(0)},$$

$$Q_2^{(0)} = (\varphi^n)^{(0)} q_3 c_2^{(0)} - (\varphi^n)^{(0)} (\varphi^f)^{(0)} q_4 c_1^{(0)} c_2^{(0)},$$

$$\Sigma^{(0)} = \frac{\left( (\varphi^f)^{(0)} - \varphi^* \right)}{\left( 1 - (\varphi^f)^{(0)} \right)^2} \mathcal{H}((\varphi^f)^{(0)} - \varphi^*),$$

$$\Lambda^{(0)} = \frac{\chi}{1 + \left( \kappa c_2^{(0)} \right)^m}.$$

## Appendix B: $\mathcal{O}(q_1)$ coefficients

$$(\varphi^n)^{(1)} = -(\varphi^f)^{(1)},$$

$$\begin{aligned} \Upsilon^f{}^{(1)} &= \left( (\varphi^f)^{(0)} (\varphi^n)^{(1)} + (\varphi^f)^{(1)} (\varphi^n)^{(0)} \right) \frac{s_0 c_2^{(0)}}{1 + s_1 c_2^{(0)}} + (\varphi^f)^{(0)} (\varphi^n)^{(0)} \left( \frac{s_0 c_2^{(1)}}{1 + s_1 c_2^{(0)}} - \frac{s_0 s_1 c_2^{(0)} c_2^{(1)}}{\left( 1 + s_1 c_2^{(0)} \right)^2} \right) \\ &\quad + \left( (\varphi^f)^{(0)} (\varphi^n)^{(1)} + (\varphi^f)^{(1)} (\varphi^n)^{(0)} \right) \frac{s_2 c_1^{(0)}}{1 + s_3 c_1^{(0)}} + (\varphi^f)^{(0)} (\varphi^n)^{(0)} \left( \frac{s_2 c_1^{(1)}}{1 + s_3 c_1^{(0)}} - \frac{s_2 s_3 c_1^{(0)} c_1^{(1)}}{\left( 1 + s_3 c_1^{(0)} \right)^2} \right) \\ &\quad - \left( (\varphi^f)^{(1)} \frac{s_4 + s_5 c_1^{(0)}}{1 + s_6 c_1^{(0)}} + (\varphi^f)^{(0)} \left( \frac{s_5 c_1^{(1)}}{1 + s_6 c_1^{(0)}} - \frac{s_6 c_1^{(1)} (s_4 + s_5 c_1^{(0)})}{\left( 1 + s_6 c_1^{(0)} \right)^2} \right) \right) \mathcal{H}(c_1^{(1)} - c_1^*), \end{aligned}$$

$$\begin{aligned} Q_1^{(1)} &= (\varphi^f)^{(0)} (\varphi^n)^{(0)} q_0 \left( c_1^{(1)} - (c_1^{(0)})^2 \right) + \left( (\varphi^f)^{(0)} (\varphi^n)^{(1)} + (\varphi^f)^{(1)} (\varphi^n)^{(0)} \right) q_0 c_1^{(0)} - (\varphi^f)^{(0)} (\varphi^n)^{(0)} q_2 c_1^{(1)} \\ &\quad - \left( (\varphi^f)^{(0)} (\varphi^n)^{(1)} + (\varphi^f)^{(1)} (\varphi^n)^{(0)} \right) q_2 c_1^{(0)}, \end{aligned}$$

$$\begin{aligned} Q_2^{(1)} &= q_3 \left( (\varphi^n)^{(0)} c_2^{(1)} + (\varphi^n)^{(1)} c_2^{(0)} \right) - q_4 \left( (\varphi^n)^{(0)} (\varphi^f)^{(1)} + (\varphi^n)^{(1)} (\varphi^f)^{(0)} \right) c_1^{(0)} c_2^{(0)} \\ &\quad - q_4 (\varphi^n)^{(0)} (\varphi^f)^{(0)} \left( c_1^{(0)} c_2^{(1)} + c_1^{(1)} c_2^{(0)} \right), \end{aligned}$$

$$\Sigma^{(1)} = \left( \frac{(\varphi^f)^{(1)}}{\left( 1 - (\varphi^f)^{(0)} \right)^2} + \frac{2 \left( (\varphi^f)^{(0)} - \varphi^* \right) (\varphi^f)^{(1)}}{\left( 1 - (\varphi^f)^{(0)} \right)^3} \right) \mathcal{H}((\varphi^f)^{(1)} - \varphi^*),$$

$$\Lambda^{(1)} = -\frac{m\chi\kappa^m \left(c_2^{(0)}\right)^{m-1} c_2^{(1)}}{\left(1 + \kappa^m \left(c_2^{(0)}\right)^m\right)^2}.$$

## References

- Ahmed IU, Byrne HM, Myerscough MR (2023) Macrophage anti-inflammatory behaviour in a multiphase model of atherosclerotic plaque development. *Bulletin of Mathematical Biology* 85(5):37
- Alam M, Dey B, Sekhar GR (2019) Mathematical modeling and analysis of hydroelastodynamics inside a solid tumor containing deformable tissue. *ZAMM-Journal of Applied Mathematics and Mechanics/Zeitschrift für Angewandte Mathematik und Mechanik* 99(5):e201800223
- Berliner JA, Navab M, Fogelman AM, et al (1995) Atherosclerosis: basic mechanisms: oxidation, inflammation, and genetics. *Circulation* 91(9):2488–2496
- Bonithon-Kopp C, Touboul PJ, Berr C, et al (1996) Relation of intima-media thickness to atherosclerotic plaques in carotid arteries: the vascular aging (eva) study. *Arteriosclerosis, Thrombosis, and Vascular biology* 16(2):310–316
- van den Bos E, Walbaum S, Horsthemke M, et al (2020) Time-lapse imaging of mouse macrophage chemotaxis. *Journal of Visualized Experiments* (158):e60750
- Breward C, Byrne H, Lewis C (2002) The role of cell-cell interactions in a two-phase model for avascular tumour growth. *Journal of Mathematical Biology* 45(2):125–152
- Breward CJ, Byrne HM, Lewis CE (2003) A multiphase model describing vascular tumour growth. *Bulletin of Mathematical Biology* 65(4):609–640
- Byrne H, Preziosi L (2003) Modelling solid tumour growth using the theory of mixtures. *Mathematical medicine and biology: a journal of the IMA* 20(4):341–366
- Byrne HM, King JR, McElwain DS, et al (2003) A two-phase model of solid tumour growth. *Applied Mathematics Letters* 16(4):567–573
- Calvez V, Ebde A, Meunier N, et al (2009) Mathematical modelling of the atherosclerotic plaque formation. In: *Esaim: Proceedings, EDP Sciences*, pp 1–12
- Calvez V, Houot JG, Meunier N, et al (2010) Mathematical and numerical modeling of early atherosclerotic lesions. In: *ESAIM: Proceedings, EDP Sciences*, pp 1–14
- Chalmers AD, Cohen A, Bursill CA, et al (2015) Bifurcation and dynamics in a mathematical model of early atherosclerosis. *Journal of Mathematical Biology* 71(6):1451–1480

- Chalmers AD, Bursill CA, Myerscough MR (2017) Nonlinear dynamics of early atherosclerotic plaque formation may determine the efficacy of high density lipoproteins (hdl) in plaque regression. *PLoS One* 12(11):e0187674
- Channon KM (2006) The endothelium and the pathogenesis of atherosclerosis. *Medicine* 34(5):173–177
- Chatzizisis YS, Coskun AU, Jonas M, et al (2007) Role of endothelial shear stress in the natural history of coronary atherosclerosis and vascular remodeling: molecular, cellular, and vascular behavior. *Journal of the American College of Cardiology* 49(25):2379–2393
- Chen D, Roda JM, Marsh CB, et al (2012) Hypoxia inducible factors-mediated inhibition of cancer by gm-csf: a mathematical model. *Bulletin of Mathematical Biology* 74(11):2752–2777
- Cilla M, Pena E, Martinez MA (2014) Mathematical modelling of atheroma plaque formation and development in coronary arteries. *Journal of The Royal Society Interface* 11(90):20130866
- Cobbold C, Sherratt J, Maxwell S (2002) Lipoprotein oxidation and its significance for atherosclerosis: a mathematical approach. *Bulletin of Mathematical Biology* 64(1):65–95
- Cohen A, Myerscough MR, Thompson RS (2014) Athero-protective effects of high density lipoproteins (hdl): an ode model of the early stages of atherosclerosis. *Bulletin of Mathematical Biology* 76(5):1117–1142
- Cunningham KS, Gotlieb AI (2005) The role of shear stress in the pathogenesis of atherosclerosis. *Laboratory Investigation* 85(1):9–23
- Davies M, Woolf N (1993) Atherosclerosis: what is it and why does it occur? *British Heart Journal* 69(1 Suppl):S3
- Dey B, Raja Sekhar GP (2016) Hydrodynamics and convection enhanced macromolecular fluid transport in soft biological tissues: Application to solid tumor. *Journal of Theoretical Biology* 395:62–86
- Dey B, Sekhar GR, Mukhopadhyay SK (2018) In vivo mimicking model for solid tumor towards hydromechanics of tissue deformation and creation of necrosis. *Journal of biological physics* 44:361–400
- El Khatib N, Génieys S, Volpert V (2007) Atherosclerosis initiation modeled as an inflammatory process. *Mathematical Modelling of Natural Phenomena* 2(2):126–141
- El Khatib N, Génieys S, Kazmierczak B, et al (2009) Mathematical modelling of atherosclerosis as an inflammatory disease. *Philosophical Transactions of the Royal*

- Society A: Mathematical, Physical and Engineering Sciences 367(1908):4877–4886
- El Khatib N, Génieys S, Kazmierczak B, et al (2012) Reaction–diffusion model of atherosclerosis development. *Journal of Mathematical Biology* 65(2):349–374
- Filipovic N, Teng Z, Radovic M, et al (2013) Computer simulation of three-dimensional plaque formation and progression in the carotid artery. *Medical & Biological Engineering & computing* 51(6):607–616
- Furchgott RF (1999) Endothelium-derived relaxing factor: discovery, early studies, and identification as nitric oxide. *Bioscience Reports* 19(4):235–251
- Grootaert MO, da Costa Martins PA, Bitsch N, et al (2015) Defective autophagy in vascular smooth muscle cells accelerates senescence and promotes neointima formation and atherogenesis. *Autophagy* 11(11):2014–2032
- Gui T, Shimokado A, Sun Y, et al (2012) Diverse roles of macrophages in atherosclerosis: from inflammatory biology to biomarker discovery. *Mediators of Inflammation* 2012
- Han K, Hong K, Park J, et al (2004) Crp promotes mcp-1 mediated chemotaxis through upregulating ccr2 expression in human monocytes. *Circulation* 109:2566–2571
- Hansson GK, Libby P (2006) The immune response in atherosclerosis: a double-edged sword. *Nature Reviews Immunology* 6(7):508–519
- Hansson GK, Robertson AKL, Söderberg-Nauclér C (2006) Inflammation and atherosclerosis. *Annual Review of Pathology: Mechanisms of Disease* 1:297–329
- Hao W, Friedman A (2014) The ldl-hdl profile determines the risk of atherosclerosis: a mathematical model. *PloS One* 9(3):e90497
- Hegy L, Skepper JN, CARY NR, et al (1996) Foam cell apoptosis and the development of the lipid core of human atherosclerosis. *The Journal of Pathology* 180(4):423–429
- Hillen T, Painter KJ (2009) A user’s guide to pde models for chemotaxis. *Journal of Mathematical Biology* 58(1):183–217
- Hoffmann KA, Chiang ST (2000) Computational fluid dynamics volume i. Engineering Education System
- Hubbard M, Byrne H (2013) Multiphase modelling of vascular tumour growth in two spatial dimensions. *Journal of theoretical biology* 316:70–89
- Ibragimov A, McNeal C, Ritter L, et al (2005) A mathematical model of atherogenesis as an inflammatory response. *Mathematical Medicine and Biology* 22(4):305–333

- Kim Y, Friedman A (2010) Interaction of tumor with its micro-environment: A mathematical model. *Bulletin of Mathematical Biology* 72(5):1029–1068
- Korshunov VA, Schwartz SM, Berk BC (2007) Vascular remodeling: hemodynamic and biochemical mechanisms underlying glagov's phenomenon. *Arteriosclerosis, Thrombosis, and Vascular Biology* 27(8):1722–1728
- Kumar P, Dey B, Raja Sekhar GP (2018) Nutrient transport through deformable cylindrical scaffold inside a bioreactor: an application to tissue engineering. *International Journal of Engineering Science* 127:201–216
- Lee T, Baines MJ, Langdon S, et al (2013) A moving mesh approach for modelling avascular tumour growth. *Applied Numerical Mathematics* 72:99–114
- Lemon G, King JR, Byrne HM, et al (2006) Mathematical modelling of engineered tissue growth using a multiphase porous flow mixture theory. *Journal of Mathematical Biology* 52(5):571–594
- Libby P, Ridker PM, Maseri A (2002) Inflammation and atherosclerosis. *Circulation* 105(9):1135–1143
- Liu LK, Lee HJ, Shih YW, et al (2008) Mulberry anthocyanin extracts inhibit ldl oxidation and macrophage-derived foam cell formation induced by oxidative ldl. *Journal of Food Science* 73(6):H113–H121
- Lusis A (2000) Atherosclerosis. *Nature* 407(6801):233–241
- Marchant CE, Van Der Wen C, Law NS, et al (1996) Oxidation of low-density lipoprotein by human monocyte-macrophages results in toxicity to the oxidising culture. *Free Radical Research* 24(5):333–342
- McKay C, McKee S, Mottram N, et al (2005) Towards a model of atherosclerosis. University of Strathclyde pp 1–29
- Meyer G, Merval Rg, Tedgui A (1996) Effects of pressure-induced stretch and convection on low-density lipoprotein and albumin uptake in the rabbit aortic wall. *Circulation Research* 79(3):532–540
- Mow VC, Holmes MH, Lai WM (1984) Fluid transport and mechanical properties of articular cartilage: a review. *Journal of Biomechanics* 17(5):377–394
- Navab M, Ananthramaiah G, Reddy ST, et al (2004) Thematic review series: the pathogenesis of atherosclerosis the oxidation hypothesis of atherogenesis: the role of oxidized phospholipids and hdl. *Journal of Lipid Research* 45(6):993–1007
- Newby AC, Zaltsman AB (1999) Fibrous cap formation or destruction—the critical importance of vascular smooth muscle cell proliferation, migration and matrix formation. *Cardiovascular Research* 41(2):345–360

- Ougrinovskaia A, Thompson RS, Myerscough MR (2010) An ode model of early stages of atherosclerosis: mechanisms of the inflammatory response. *Bulletin of Mathematical Biology* 72(6):1534–1561
- Prakash J, Raja Sekhar GP, De S, et al (2010) A criterion to avoid starvation zones for convection–diffusion–reaction problem inside a porous biological pellet under oscillatory flow. *International Journal of Engineering Science* 48(7-8):693–707
- Pramanik AS, Dey B, Karmakar T, et al (2023) Two-phase modeling of fluid injection inside subcutaneous layer of skin. *International Journal of Engineering Science* 192:103935
- Ross R (1999) Atherosclerosis—an inflammatory disease. *New England Journal of Medicine* 340(2):115–126
- Roth GA, Abate D, Abate KH, et al (2018) Global, regional, and national age-sex-specific mortality for 282 causes of death in 195 countries and territories, 1980–2017: a systematic analysis for the global burden of disease study 2017. *The Lancet* 392(10159):1736–1788
- Stangeby DK, Ethier CR (2002) Coupled computational analysis of arterial ldl transport—effects of hypertension. *Computer Methods in Biomechanics & Biomedical Engineering* 5(3):233–241
- Watson MG, Byrne HM, Macaskill C, et al (2018) A two-phase model of early fibrous cap formation in atherosclerosis. *Journal of Theoretical Biology* 456:123–136
- Watson MG, Byrne HM, Macaskill C, et al (2020) A multiphase model of growth factor-regulated atherosclerotic cap formation. *Journal of Mathematical Biology* 81(2):725–767
- Wu MY, Li CJ, Hou MF, et al (2017) New insights into the role of inflammation in the pathogenesis of atherosclerosis. *International Journal of Molecular Sciences* 18(10):2034
- Zaman A, Ali N, Bég OA (2016) Unsteady magnetohydrodynamic blood flow in a porous-saturated overlapping stenotic artery—numerical modeling. *Journal of Mechanics in Medicine and Biology* 16(04):1650049
- Zheng C, Yang Q, Cao J, et al (2016) Local proliferation initiates macrophage accumulation in adipose tissue during obesity. *Cell death & disease* 7(3):e2167–e2167